Big Data and Neural Networks in Smart Grid - Part 1: The Impact of Measurement Differences on the Performance of Neural Network Identification Methodologies of Overhead Low-Voltage Broadband over Power Lines Networks

Athanasios G. Lazaropoulos[1,2,*] and Helen C. Leligou[2]

1: School of Electrical and Computer Engineering / National Technical University of Athens / 9 Iroon Polytechniou Street / Zografou, GR 15780
2: Department of Industrial Design and Production Engineering / School of Engineering / University of West Attica / 250 Thivon & P. Ralli / Athens, GR 12244

Until now, the neural network identification methodology for the branch number identification (NNIM-BNI) and the neural network identification methodology for the distribution line and branch line length approximation (NNIM-LLA) have approximated the number of branches and the distribution line and branch line lengths given the theoretical channel attenuation behavior of the examined overhead low-voltage broadband over powerlines (OV LV BPL) topologies [1], [2]. The impact of measurement differences that follow continuous uniform distribution (CUDs) of different intensities on the performance of NNIM-BNI and NNIM-LLA is assessed in this paper. The countermeasure of the application of OV LV BPL topology databases of higher accuracy is here investigated in the case of NNIM-LLA. The strong inherent mitigation efficiency of NNIM-BNI and NNIM-LLA against CUD measurement differences and especially against those of low intensities is the key finding of this paper. The other two findings that are going to be discussed in this paper are: (i) The dependence of the approximation Root-Mean-Square Deviation (RMSD) stability of NNIM-BNI and NNIM-LLA on the applied default operation settings; and (ii) the proposal of more elaborate countermeasure techniques from the literature against CUD measurement differences aiming at improving NNIM-LLA approximations.

1. Introduction

During the recent years, the evolution of the traditional power grid, which represents an omnipresent widely branched hierarchical network structure with relatively few one-way communications modalities, to a modern power grid that is upgraded with an intelligent IP-based communications network of two-way information flows may support a myriad of broadband applications [1]-[9]. The supported broadband applications can facilitate the today's digital transformation of power utilities and consumers, namely: (i) power utilities' operations and management -e.g., real-time

monitor, meter and control of the power grid equipment and wired infrastructure-; and (ii) customers' needs and demands -e.g., real-time monitor and control of their power flows-. To implement the two-way information flow across the smart grid, Broadband over Power Lines (BPL) networks exploit the available wired power grid infrastructure while permitting their integration with other communications solutions, such as Radio Frequency (RF) mesh, modified Long Term Evolution (LTE), Code Division Multiple Access (CDMA) at sub GHz bands, dedicated fiber along high voltage lines and 5G communications, through their BPL wireline / wireless interfaces [3], [7], [8], [10].

A plethora of channel models has been applied for characterizing BPL channels; say, deterministic, statistical, bottom-up, top-down, hybrid BPL channel models and. more recently, BPL channel models that exploit artificial intelligence (AI), machine learning (ML) and neural network (NN) capabilities [1], [11]-[26]. On the basis of the deterministic hybrid model (DHM) of [1], [2], which describes BPL signal propagation and transmission across the topologies of the overhead low voltage (OV LV) BPL networks, critical DHM broadband performance metrics, such as the channel attenuation of the OV LV BPL topologies, may be further exploited by the BPL broadband applications of the smart grid. Indeed, Topology Identification Methodology (TIM), which has been proposed in [27], [28] and is among the BPL broadband applications of the smart grid, can approximate the exact topological characteristics (*i.e.*, number of branches, length of branches, length of main lines and branch terminations) of an examined BPL topology by comparing the available channel attenuation measurements of the examined BPL topology with the theoretical DHM channel attenuation results of various OV LV BPL topologies stored in the TIM BPL topology database. By exploiting the available big data of the TIM BPL topology database for the OV LV BPL topologies and AI - ML - NN capabilities, the neural network identification methodology for the branch number identification (NNIM-BNI) and the neural network identification methodology for the distribution line and branch line length approximation (NNIM-LLA) have been proposed for the OV LV BPL topologies in [1] and [2], respectively. More specifically, NNIM-BNI aims at identifying the number of branches and NNIM-LLA tries to approximate the distribution line and branch line lengths for a given OV LV BPL topology *theoretical* channel attenuation behavior when the corresponding OV LV BPL topology does not lie among the ones of the TIM BPL topology database in both methodology cases.

However, measurement differences between experimental and theoretical OV LV BPL topology channel attenuation values may occur due to several practical reasons and "real" life conditions while these measurement differences may significantly affect the performance of the BPL broadband applications of the smart grid [28]-[32]. In this paper, the effect of the measurement differences observed between the experimental and theoretical OV LV BPL topology channel attenuation values on the performance of NNIM-BNI and NNIM-LLA is first assessed. In accordance with [28], [29], [32], [33], a typical scenario to take into account the measurement differences during the BPL topology channel attenuation analysis is their handling as error distributions such as Continuous Uniform Distributions (CUDs) and Normal Distributions (NDs) that are superimposed to the coupling scheme transfer function theoretical numerical results of DHM. In this paper, measurement differences are going to be simulated as CUDs of various intensities. The procedure that is going to be followed so as to assess the impact of measurement differences as CUDs on the NNIM-BNI and NNIM-LLA approximation performance consists of two Phases, namely: (i) *Phase 1*: Exploiting the list of indicative

OV LV BPL topologies of [1], [2], the representative database sets of the TIM OV LV BPL topology database and the default operation settings A presented in [1], the branch number approximations of NNIM-BNI are compared against the corresponding best branch number approximation without measurement differences and the real branch number for given indicative OV LV BPL topology when CUD measurement differences of various intensities are assumed; and (ii) *Phase 2*: Focusing on the same list of indicative OV LV BPL topologies of [1], [2], the default operation settings B of [2], are here applied. In order to improve the NNIM-LLA performance and cope with the insidious effect of measurement differences, the default operation settings C, that are a more elaborate version of the default operation settings B of [2], are here proposed as a fine countermeasure against measurement differences. First, the NNIM-LLA approximations of the distribution line and branch line lengths, when CUD measurement differences of various intensities and default operation settings B are assumed, are compared against the corresponding approximations without measurement differences of default operation settings B so that the performance of NNIM-LLA is assessed against the measurement differences. Second, the performance of NNIM-LLA approximations of the distribution line and branch line lengths is benchmarked when CUD measurement differences of the same intensities and default operation settings C are assumed. Here, the role of the default operation settings of higher accuracy against the CUD measurement differences is investigated. In accordance with [1], [2], the performance metric that is going to be applied in both Phases of this paper is the Root-Mean-Square Deviation (RMSD) so that the impact of the CUD measurement differences on the NNIM-BNI and NNIM-LLA approximation performance can be assessed. Conversely to [1], [2], it should be noted that the theoretical channel attenuation measurements of the examined OV LV BPL topologies will be included in the TIM BPL topology database of this paper as well as the topological characteristics of the corresponding OV LV BPL topologies.

The rest of this paper is organized as follows: Section 2 briefly presents DHM, NNIM-BNI and NNIM-LLA. Certain aspects that highlight the operation points of NNIM-BNI and NNIM-LLA, which are vulnerable to measurement differences, are presented in this Section. In addition, the mathematics concerning the involvement of measurement differences during the NNIM-BNI and NNIM-LLA operation are reported. In Section 3, the numerical results regarding the impact of measurement differences on the approximation performance of NNIM-BNI and NNIM-LLA are given. Section 4 concludes this paper.

2. DHM, TIM OV LV BPL Topology Database, NNIM-BNI and NNIM-LLA

In this Section, DHM and TIM OV LV BPL topology database that are responsible for the big data pool of NNIM-BNI and NNIM-LLA are first presented in this Section. Here, DHM is presented by focusing on its output of OV LV BPL topology channel attenuation that is appropriately included into TIM OV LV BPL topology database as the theoretical coupling scheme channel transfer functions. Also, the effect of CUD measurement differences on the DHM output is mathematically presented. Second, NNIM-BNI and NNIM-LLA, which have been proposed in [1] and [2], respectively, are briefly discussed as well as the corresponding useful conclusions of [1], [2] that are going to be exploited in this pair of papers and may further affect the operation and performance of NNIM-BNI and NNIM-LLA.

2.1 DHM and the Mathematics of the Measurement Differences

DHM is a synthetic BPL channel model of three concatenated modules; say, the bottom-up, the top-down and the coupling scheme modules [1], [2], [9], [11]-[13], [34]-[36]. More specifically, the bottom-up and top-down modules of DHM address the propagation and transmission issues of the BPL signal across the OV LV BPL topologies. To deal with the aforementioned propagation / transmission problem, the bottom-up and top-down modules of DHM require details about the applied OV LV Multi-conductor Transmission Line (MTL) configurations and the OV LV BPL topologies, namely:

1. As the OV LV MTL configuration that is applied in this paper is concerned, the typical OV LV MTL configuration of Fig. 1(a) is assumed. The examined OV LV MTL configuration consists of four parallel non-insulated conductors (i.e., $n^{\text{OVLV}} = 4$) of vertical distance that is equal to Δ_{OVLV}. The upper conductor of radius $r_{\text{OVLV,n}}$ is the neutral conductor while the lower three conductors of radius $r_{\text{OVLV,p}}$ are the three LV phases. The lowest phase conductor is hung at height h_{OVLV} above the ground. The exact dimensions, the material of the conductors and the structure of the conductors are detailed in [9], [11], [13], [15], [37], [38]. The reference conductor of the OV LV MTL configuration is assumed to be the imperfect lossy ground of properties reported in [39]-[41].

2. As the OV LV BPL topologies that are used in this paper are concerned, the typical OV LV BPL topology of Fig. 1(b) is assumed. With reference to Fig. 1(b), the typical OV LV BPL topology is bounded by the transmitting and receiving ends while N branches of open-circuit terminations are encountered across the transmitting path. The arbitrary k, $k=1,\ldots,N$ branch has length equal to $L_{\text{b}k}$ and is located at distance $\sum_{i=1}^{k} L_i$ from the transmitting end. The same length $\sum_{i=1}^{N+1} L_i$ of 1000m is assumed between the transmitting and receiving ends for all the applied OV LV BPL topologies of this paper [1], [25]. In accordance with [1], [2], [13], [34] the topological characteristics and the number of branches for five indicative OV LV BPL topologies –i.e., Line-Of-Sight (LOS), rural, suburban, urban A and urban B– are listed in Table 1. The indicative OV LV BPL topologies that are included in Table 1 may offer a general study of all OV LV BPL topology classes that are encountered in BPL networks. The indicative OV LV BPL topologies of Table 1 have already been used as OV LV BPL topology case studies during the benchmark of TIM-BNI, NNIM-BNI, TIM-LLA and NNIM-LLA in [1], [26].
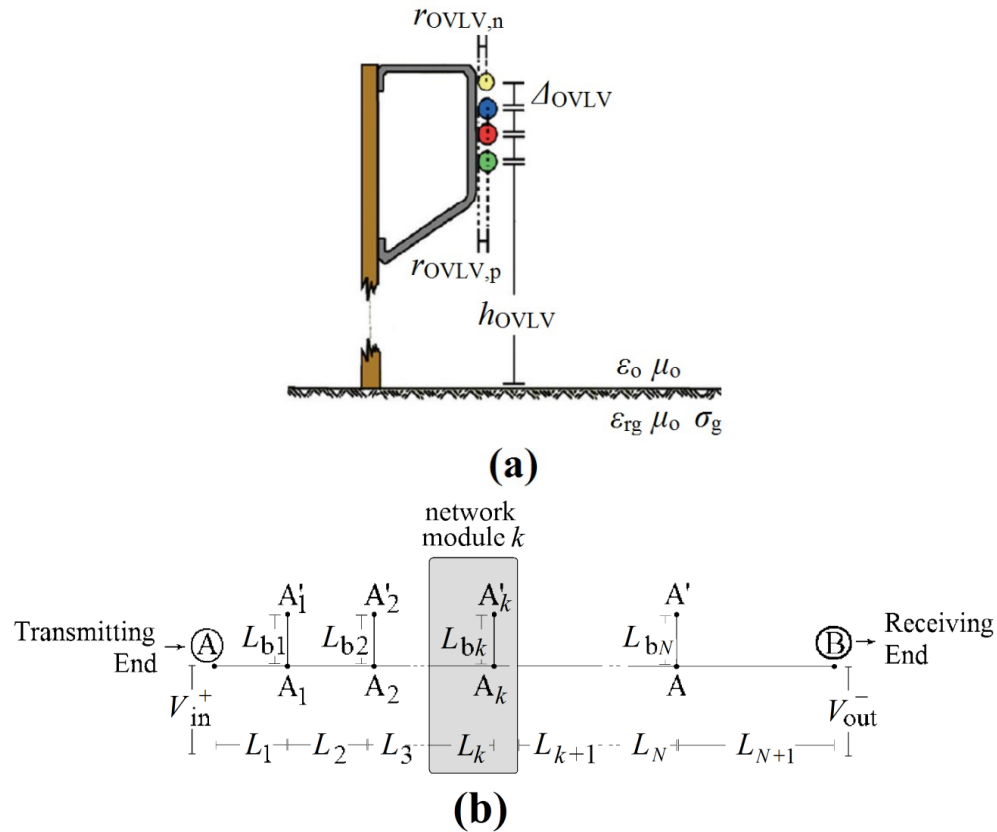
Figure 1. (a) OV LV MTL configuration [1], [9], [13]. (b) Typical OV LV BPL topology with *N* branches [1], [25].

Table 1
Indicative OV LV BPL Topologies [1], [13], [26], [34]

OV LV BPL Topology Name	Branch Number (*N*)	Length of Main Lines	Length of Branches
Urban case A (Typical urban case)	3	L_1=500m, L_2=200m, L_3=100m, L_4=200m	L_{b1}=8m, L_{b2}=13m, L_{b3}=10m
Urban case B (Aggravated urban case)	5	L_1=200m, L_2=50m, L_3=100m, L_4=200m, L_5=300m, L_6=150m	L_{b1}=12m, L_{b2}=5m, L_{b3}=28m, L_{b4}=41m, L_{b5}=17m
Suburban case	2	L_1=500m, L_2=400m, L_3=100m	L_{b1}=50m, L_{b2}=10m
Rural case	1	L_1=600m, L_2=400m	L_{b1}=300m
LOS case	0	L_1=1000m	-

By the interconnection of the bottom-up and the top-down modules of DHM, the $n^{\text{OVLV}} \times n^{\text{OVLV}}$ line channel transfer function matrix $\mathbf{H}^{\text{OVLV}}\{\cdot\}$ of the typical OV LV BPL topology of Fig. 1(b) is given by [1], [2], [9], [11]-[13], [34]-[36]

$$\mathbf{H}^{\text{OVLV}}\{\cdot\} = \mathbf{T}_V^{\text{OVLV}} \cdot \mathbf{H}^{\text{OVLV,m}}\{\cdot\} \cdot \left(\mathbf{T}_V^{\text{OVLV}}\right)^{-1} \tag{1}$$

where $\mathbf{H}^{\text{OVLV,m}}\{\cdot\}$ is the $n^{\text{OVLV}} \times n^{\text{OVLV}}$ modal channel transfer function matrix and $\mathbf{T}_V^{\text{OVLV}}$ is the $n^{\text{OVLV}} \times n^{\text{OVLV}}$ transformation matrix. With reference to [1], [2], [9], [11]-[13], [34]-[36] and observing eq. (1), the line channel transfer function matrix depends on the examined OV LV MTL configuration (i.e., physical properties and geometry of the OV LV MTL configuration) and the examined OV LV BPL topology.

By the concatenation of the bottom-up and the top-down modules with the coupling scheme module of DHM, the theoretical coupling scheme channel transfer function is given by [42], [43]

$$H^{\text{OVLV,}C}\{\cdot\} = [\mathbf{C}^{\text{out}}]^{\text{OVLV,}C} \cdot \mathbf{H}^{\text{OVLV}}\{\cdot\} \cdot [\mathbf{C}^{\text{in}}]^{\text{OVLV,}C} \tag{2}$$

for given coupling scheme where $[\cdot]^c$ denotes the applied coupling scheme, $\mathbf{C}^{\text{in}}$ is the input coupling $n^{\text{OVLV}} \times 1$ column vector dealing with the BPL signal injection process and $\mathbf{C}^{\text{out}}$ is the ouput coupling $1 \times n^{\text{OVLV}}$ line vector dealing with the BPL signal extraction process. Actually, the coupling scheme channel transfer function of eq. (2) relates the output BPL signal $V^{\text{out,}-}$ with the input one $V^{\text{in,}+}$ of Fig. 1(b). It should be noted that the coupling scheme transfer function of eq. (2) is a frequency dependent function due to the involved frequency dependent function elements from eq. (1) (i.e., the modal channel transfer function and the transformation matrices) and also depends on the applied coupling scheme for the BPL signal injection / extraction across the examined OV LV BPL topology. It should be noted that the theoretical coupling scheme channel transfer function of eq. (2) is of interest for the preparation of the TIM OV LV BPL topology database of the next subsection of this paper since for given OV LV MTL configuration and coupling scheme, the corresponding theoretical coupling scheme channel transfer functions can be computed by DHM and stored in the TIM OV LV BPL topology database by only adjusting the topological characteristics of OV LV BPL topologies. With reference to [42], [43], it should be noted that the applied coupling scheme is the WtG[1] one.

The computation of the DHM coupling scheme transfer function of eq. (2) is a rather theoretical issue since no measurement differences are taken into account. However, a set of practical reasons and "real life" conditions, which can be grouped into six categories [28], [30], [44], [45], can create measurement differences during the practical determination of the coupling scheme transfer function. To assess the effect of the measurement differences during the determination of the coupling scheme transfer functions of the OV LV BPL topologies, in accordance with [28], [30], [44], [45] and with reference to eq. (2), the measured coupling scheme transfer function $\overline{H_{d1,d2,i}^{\text{OVLV,}C,D}}\{\cdot\}$ is determined by

$$\overline{H_{d1,d2,i}^{\text{OVLV,}C,D}}(f_q) = H^{\text{OVLV,}C}(f_q) + e_{d1,d2,i}^{D}(f_q), q=1,\ldots,Q, \; i = 1,\ldots,I \tag{3}$$

where $[\cdot]^D$ denotes the applied measurement difference distribution (i.e., CUD in this paper), $d1$ is the first parameter of the applied measurement difference distribution (i.e., the minimum value $-a_{\text{CUD}}$ of CUD in this paper), $d2$ is the second parameter of the applied measurement difference distribution (i.e., the maximum value a_{CUD} of CUD in this paper), $e_{d1,d2,i}^{D}(f_q)$ is the measurement difference at frequency f_q for given measurement difference distribution, I is the number of different $1 \times Q$ line vectors of

measurement differences per applied measurement difference distribution, first and second parameter and i indicates the ith among I line vectors of measurement differences. In this paper, 1 representative line vector of measurement differences are going to be assumed per applied measurement difference distribution, first and second parameter; say, $i=I=1$. It should be noted that the measured coupling scheme channel transfer function of eq. (3) is of interest for the NNIM-BNI and NNIM-LLA since for given OV LV MTL configuration and coupling scheme, the corresponding I measured coupling scheme channel transfer functions are approximated in terms of the branch number and main / branch line lengths.

2.2 TIM OV LV BPL Topology Database

In accordance with [1], [2], TIM OV LV BPL topology database acts as the big data pool for NNIM-BNI and NNIM-LLA. In fact, TIM OV LV BPL topology database is the core part of TIM and is borrowed by the NNIM-based methodologies due to its big data detail concerning the correspondence among topological characteristics and coupling scheme transfer function behavior of the OV High-Voltage (HV), Medium-Voltage (MV) and LV topologies [27]. Combining the database requirements of [1], [2], TIM OV LV BPL topology database consists of the following fields for each OV LV BPL topology: (i) the ID number p of the OV LV BPL topology when the number of all OV LV BPL topologies in the TIM OV LV BPL topology database is equal to P; (ii) the actual number of branches N of the OV LV BPL topology; (iii) the actual lengths of the distribution lines $\mathbf{L} = [L_1 \quad L_2 \quad \cdots \quad L_{N+1}]$ of the OV LV BPL topology; (iv) the actual lengths of the branch lines $\mathbf{L_b} = [L_{b1} \quad L_{b2} \quad \cdots \quad L_{bN}]$ of the OV LV BPL topology; and (v) the theoretical coupling scheme channel transfer function values with respect to the frequency of the OV LV BPL topology as given in eq. (2). The size of the TIM OV LV BPL topology database depends on the default operation settings that are applied during its preparation (see Sec. 2.3).

2.3 Default Operation Settings

With reference to [1], [2], the applied default operation settings have a direct impact on the size of the TIM OV LV BPL topology database and, thus, on the performance of the NNIM-based methodologies. Actually, the default operation settings define the values of the maximum number of branches N_{max}, the length spacing L_s for both the branch distance and the branch length, the maximum branch length $L_{b,max}$ and the operation frequency range that are anyway essential factors for the five fields of TIM OV LV BPL topology database [27], [28]. The following values of the default operation settings of this paper are concerned, namely:

- *The Default Operation Settings A for NNIM-BNI*: In accordance with [1], the number of branches for the OV LV BPL topologies of the TIM OV LV BPL topology database ranges from 0 (say, "LOS" case of Table 1) up to 3 branches (say, urban case A of Table 1). The length spacings for the branch distance and the branch length are assumed to be equal to 100m and 25m, respectively, while the branch line length may range from 0m to 100m. Note that the total distribution line length is assumed to be equal to 1,000m in all the OV LV BPL topologies of the TIM OV LV BPL topology database. The amplitudes of the coupling scheme channel transfer functions in dB are stored in the TIM OV LV BPL topology database for the OV LV BPL topologies with respect to the frequency. The frequency range is assumed to be equal to 3-30MHz while the flat-fading

subchannel frequency spacing is equal to 1MHz. In accordance with [1], representative sets of the TIM OV LV BPL topology database (database representativeness) are assumed during the operation of the NNIM-BNI for the branch number approximation of the urban case A (3 branches), suburban case (2 branches) and rural case (1 branch). Especially, in this paper, the following improvements are additionally assumed after the observation of the NNIM-BNI operation and performance of [1]: (i) The urban case A, suburban case, rural case and LOS case will be included into the TIM OV LV BPL topology database. Conversely to [1], NNIM-BNI does not blindly operate in this paper; and (ii) for NNIM-BNI branch number approximations that are not in the range from 0 (minimum acceptable branch number value) to 4 (maximum acceptable branch number value with respect to the preparation of the TIM OV LV BPL topology database), NNIM-BNI approximation is again executed.

- *The Default Operation Settings B and C for NNIM-LLA:* As the default operation settings B are concerned in [2], the number of branches for the OV LV BPL topologies of the TIM OV LV BPL topology database are going to range from 0 (say, "LOS" case) up to 2 branches in this paper due to time delay reasons regarding the application of the following default operation settings C; from [1], [2], it has been verified that the preparation time of the TIM OV LV BPL topology database exponentially increases with the increase of the demanded accuracy of the default operation settings thus establishing a relationship between the approximation performance and total duration time of the NNIM-based methodologies. The length spacings for the branch distance and the branch length are assumed to be equal to 100m and 100m, respectively, while the branch line length may range from 0m to 300m. Note that the total distribution line length is assumed to be equal to 1,000m in all the OV LV BPL topologies of the TIM OV LV BPL topology database. The amplitudes of the coupling scheme channel transfer functions in dB are stored in the TIM OV LV BPL topology database for the OV LV BPL topologies with respect to the frequency. The frequency range is assumed equal to 3-88MHz while the flat-fading subchannel frequency spacing is equal to 1MHz. By comparing default operation settings A and B, it is evident that default operation settings B are more elaborate in comparison with the default operation settings A and this is due to the fact that the approximation of the distribution line and branch line lengths remains a difficult challenge where higher accuracy is expected from the TIM OV LV BPL topology database that is going to be exploited by the NNIM-based methodology. To examine the further improvement tomography potential of NNIM-LLA and its behavior when measurement differences are applied, default operation settings C, which are proposed in this paper, are more elaborate in comparison with the default operation settings B. Anyway, the application of the default operation settings C is also examined in this paper to act as a countermeasure again the measurement differences. Hence, as the default operation settings C are concerned in this paper, the length spacings for the branch distance and the branch length are assumed to be equal to 100m and 30m, respectively, while the branch line length may range from 0m to 300m. Similarly to default operation settings B, the total distribution line length, the frequency range and the flat-fading subchannel frequency spacing are assumed to be the same. In addition, the following assumptions are made: (i) The number of branches of the examined indicative OV LV BPL topologies is

assumed to be known; and (ii) the database representativeness, which is analyzed in [2] for the operation of NNIM-LLA, is assumed during the application of the default operation settings B and C. In accordance with [2], only one of the symmetrical OV LV BPL topologies is stored in the OV LV BPL topology database so as not to disrupt the approximations due to the symmetry of BPL topologies described in [64], [46]. Especially, in this paper, the following improvements are assumed with respect to the NNIM-LLA operation and its performance of [2]: (i) The suburban case, rural case and LOS case will be included into the TIM OV LV BPL topology database in default operation settings B and C while only the distribution line and branch line lengths of the suburban case and rural case are going to be approximated by NNIM-LLA. Conversely to [2], NNIM-LLA does not blindly operate in this paper; (ii) for NNIM-LLA distribution line fragment length approximations that are not in the range from 0m (minimum acceptable distribution line length) to 1000m (total distribution line length), NNIM-LLA approximation is again executed; and (iii) for NNIM-LLA branch line fragment length approximations that are not in the range from 0m (minimum acceptable branch line length) to 150m or 300m for the default operation settings B or C, respectively (maximum acceptable branch line length), NNIM-LLA approximation is again executed. Note that the last two improvements cope with the unacceptable NNIM-LLA approximations of [2] (i.e., at least one of the approximated distribution and branch line lengths is below zero given the fixed length of 1000m between the transmitting and receiving ends for all the applied OV LV BPL topologies of this paper).

Finally, it should be noted that the default participation percentages of the three phases of NNIM-based methodologies of [1], [2], [47], [48] are assumed in this paper; say, training, validation and testing phases during the operation of NNIM-BNI and NNIM-LLA are respectively assumed to be equal to 70%, 15% and 15%.

2.4 NNIM-BNI and NNIM-LLA in a Measurement Difference Environment

NNIM-BNI lies in the research fields of AI, ML and NNs [47], [49]-[51]. NNIM-BNI has been proposed and numerically assessed in [1] against TIM-BNI, which is its alternative deterministic BNI methodology. NNIM-BNI approximates the branch numbers $N_{\mathrm{NNIM-BNI}}$ of the examined indicative OV LV BPL topology per hl hidden layer by comparing its coupling scheme channel transfer function values against the respective ones of the available OV LV BPL topologies of the TIM OV LV BPL topology database. Actually, the operation of NNIM-BNI depends on: (i) the TIM OV LV BPL topology database; and (ii) the MATLAB NN program of [47], [48] that programmatically supports the fully connected neural network architecture of Figure 2 of [1] as well as the involved training, validation and testing phases. The factors that affect the accuracy performance of the NNIM-BNI approximations and have been identified in [1] are: (i) the default operation setting values that affect the accuracy and size of the TIM OV LV BPL topology database; (ii) the representativeness of the TIM OV LV BPL topology database; (iii) the number HL of the hidden layers assumed; and (iv) the participation percentage of the three phases. Another factor that may affect the accuracy performance of the NNIM-BNI approximations when measurement differences occur is the inclusion of the examined indicative OV LV BPL topologies in the TIM OV LV BPL topology database. Until now, NNIM-BNI has exploited the performance metric of RMSD of the amplitude of the coupling scheme channel transfer function in dB, as expressed in eq. (2) since the

scenario of the existence of measurement differences is first examined in this paper. In this paper, NNIM-BNI is again going to exploit the performance metric of RMSD of the amplitude of the coupling scheme channel transfer function in dB but via the eq. (3) where measurement differences occur and are mathematically taken into account.

In [2], NNIM-BNI has been extended to NNIM-LLA so that the lengths of the distribution lines and branch lines for a given OV LV BPL topology coupling scheme channel transfer function behavior with respect to frequency can be approximated; say, NNIM-LLA achieves the tomography of the examined OV LV BPL topology. Indeed, NNIM-LLA adopts the same fully connected NN architecture of NNIM-BNI while it depends on the same factors with NNIM-BNI, say: (i) the default operation setting values that affect the TIM OV LV BPL topology database; (ii) the representativeness of the TIM OV LV BPL topology database when the number of branches for the examined OV LV BPL topology is *a priori* known; (iii) the deliberate ignorance of symmetrical OV LV BPL topologies during the preparation of the TIM OV LV BPL topology database; (iv) the number HL of the assumed hidden layers; and (v) the participation percentage of the three phases. The output of the NNIM-LLA approximates the distribution and branch line lengths of the examined indicative OV LV BPL topology (i.e., the NNIM-LLA approximation lengths of the distribution and branch lines are $\mathbf{L}_{\text{NNIM−LLA}} = [L_{1,\text{NNIM−LLA}} \quad L_{2,\text{NNIM−LLA}} \quad \cdots \quad L_{N+1,\text{NNIM−LLA}}]$ and $\mathbf{L}_{\text{b,NNIM−LLA}} = [L_{\text{b1,NNIM−LLA}} \quad L_{\text{b2,NNIM−LLA}} \quad \cdots \quad L_{\text{b}N,\text{NNIM−LLA}}]$, respectively). Similarly to NNIM-BNI, the scenario of the inclusion of the examined indicative OV LV BPL topologies in the TIM OV LV BPL topology database is first examined in this paper when measurement differences are considered. Extending the application of NNIM-LLA of [2], NNIM-LLA here exploits the performance metric of RMSD of the amplitude of the coupling scheme channel transfer function in dB when measurement differences are included, as expressed in eq. (3). In this paper, NNIM-LLA is again going to exploit the performance metric of RMSD of the amplitude of the coupling scheme channel transfer function in dB through the eq. (3) where measurement differences occur and are mathematically taken into consideration. At the NNIM-LLA output, apart from the approximation for the lengths of the distribution and branch lines, NNIM-LLA presents its approximation RMSDs per hidden layer.

3. Numerical Results and Discussion

In this Section, numerical results concerning the performance of NNIM-BNI and NNIM-LLA are presented as well as their evaluation when CUD measurement differences of different intensities are applied. The higher accuracy of the applied default operation settings is treated as the simplest countermeasure technique against measurement differences in NNIM-LLA.

3.1 NNIM-BNI – Base Scenario and Measurement Differences

As the operation of the NNIM-BNI is concerned, NNIM-BNI is based on the MATLAB NN training program of [47], [48] while the default operation settings A of Sec. 2.3 are assumed. Given the amplitudes of coupling scheme channel transfer functions in dB for the urban case A, suburban case and rural case of Table 1, NNIM-BNI gives as output in Table 2 the respective NNIM-BNI approximation of the branch

Table 2
Branch number approximation of NNIM-BNI without CUD Measurements

Indicative OV LV BPL Topologies of Table 1		Urban case A (Typical urban case)	Suburban case	Rural case	RMSD (m)	Notes
Actual Number of Branches N		**3**	**2**	**1**	**-**	-
NNIM-BNI (Approximated Number of Branches) $N_{\text{NNIM-BNI}}$	1st execution	2.67	1.80	1.13	0.24	Default Operation Settings A + 1 hidden layer
	2nd execution	3.02	2.01	1.12	0.07	
	3nd execution	3.64	2.16	1.05	0.38	
	1st execution	3.06	2.16	1.28	0.19	Default Operation Settings A + 2 hidden layers
	2nd execution	2.78	2.08	1.34	0.24	
	3nd execution	3.32	2.14	1.08	0.21	
	1st execution	2.82	1.87	1.18	0.17	Default Operation Settings A + 3 hidden layers
	2nd execution	2.78	1.97	1.21	0.18	
	3nd execution	2.06	1.78	1.44	0.61	
	1st execution	2.66	2.51	1.22	0.37	Default Operation Settings A + 4 hidden layers
	2nd execution	3.12	2.02	1.10	0.09	
	3nd execution	2.94	2.01	1.12	0.08	
	1st execution	2.99	2.08	1.10	0.08	Default Operation Settings A + 5 hidden layers
	2nd execution	2.99	2.00	1.24	0.14	
	3nd execution	3.01	2.05	1.26	0.15	

numbers $N_{\text{NNIM-BNI}}$ per hidden layer where the maximum number of hidden layers *HL* is assumed to be equal to 5. Since the results of Table 2 are going to act as the basis scenario for the effect study of measurement differences, CUD measurements are omitted in the basis scenario (i.e., a_{CUD} of CUD measurements is assumed to be equal to 0dB). Apart from the branch number approximations, the actual branch numbers of the three examined OV LV BPL topologies of Table 1 are presented for comparison reasons while the RMSDs of NNIM-BNI approximations for these three examined OV LV BPL topologies are also computed. Note that three executions of NNIM-BNI are reported for each of the three examined OV LV BPL topologies.

From Table 2, it is evident that the RMSD per hidden layer remains satisfactorily stable when different executions occur for the default operation settings A and the three examined OV LV BPL topologies of this paper. In fact, by assessing the RMSD values of Table 2, reliable NNIM-BNI approximations can occur even if 1 hidden layer and only one execution are assumed for given indicative OV LV BPL topology of Table 1. Since no CUD measurement differences are applied in the basis scenario of Table 2, the RMSD values may act as the benchmark for assessing the impact of higher a_{CUD} values of CUD measurements on the NNIM-BNI approximation performance, apart from the approximated branch numbers per OV LV BPL topology.

Similarly to Table 2, in Table 3, given the amplitudes of coupling scheme channel transfer functions contaminated with measurements in dB for the urban case A, suburban case and rural case of Table 1, NNIM-BNI gives as output the respective NNIM-BNI approximations of the branch numbers $N_{\text{NNIM-BNI}}$ when various a_{CUD} values of CUD measurements are assumed. Note that: (i) one hidden layer is assumed during the NN preparation of NNIM-BNI in this subsection; (ii) one execution is performed in each NNIM-BNI approximation case; and (iii) one measurement difference $1 \times Q = 1 \times (30 - 3) = 1 \times 27$ line vector is superimposed to the amplitudes of the coupling scheme

channel transfer functions of the aforementioned three OV LV BPL topologies in each NNIM-BNI approximation case. Apart from the branch number approximations, the actual branch numbers of the three examined OV LV BPL topologies of Table 1 are presented for comparison reasons while the RMSD values assess the approximation performance for given a_{CUD} of CUD measurements for the aforementioned BPL topologies. More analytically, to graphically examine the performance of NNIM-BNI for the various a_{CUD} values of CUD measurements of Table 3, the rounded branch number approximation of NNIM-BNI and the actual branch number are plotted in Fig. 2(a) for the urban case A with reference to Table 3. Similar figures with Fig. 2(a) are given in Figs. 2(b) and 2(c), but for the suburban and rural case of Table 3, respectively.

Table 3
Branch number approximation of NNIM-BNI for Different a_{CUD} Values of CUD Measurements

Indicative OV LV BPL Topologies of Table 1		Urban case A (Typical urban case)	Suburban case	Rural case	RMSD (m)	Notes
Actual Number of Branches N		3	2	1	-	-
NNIM-BNI (Approximated Number of Branches) $N_{NNIM-BNI}$	a_{CUD} **of CUD Measurememts (dB)**					Default Operation Settings A + 1 hidden layer
	0	2.88	1.97	1.13	0.11	
	1	3.42	2.13	1.27	0.30	
	2	3.19	2.21	1.28	0.23	
	3	3.02	1.97	0.98	0.03	
	4	2.12	1.24	0.41	0.75	
	5	2.68	1.90	0.98	0.19	
	6	2.52	2.01	1.57	0.43	
	7	3.91	2.86	1.89	0.89	
	8	2.33	1.95	1.60	0.52	
	9	2.15	1.51	1.14	0.58	
	10	2.23	2.04	1.93	0.70	
	11	2.68	1.61	0.91	0.29	
	12	2.34	1.47	0.73	0.51	
	13	3.37	1.92	1.61	0.41	
	14	2.94	2.62	2.26	0.81	
	15	1.30	0.64	0.32	1.32	
	16	2.50	2.06	1.57	0.44	
	17	2.71	1.51	0.66	0.38	
	18	2.81	2.32	1.98	0.61	
	19	1.49	1.31	0.88	0.96	
	20	2.02	0.85	0.20	0.99	
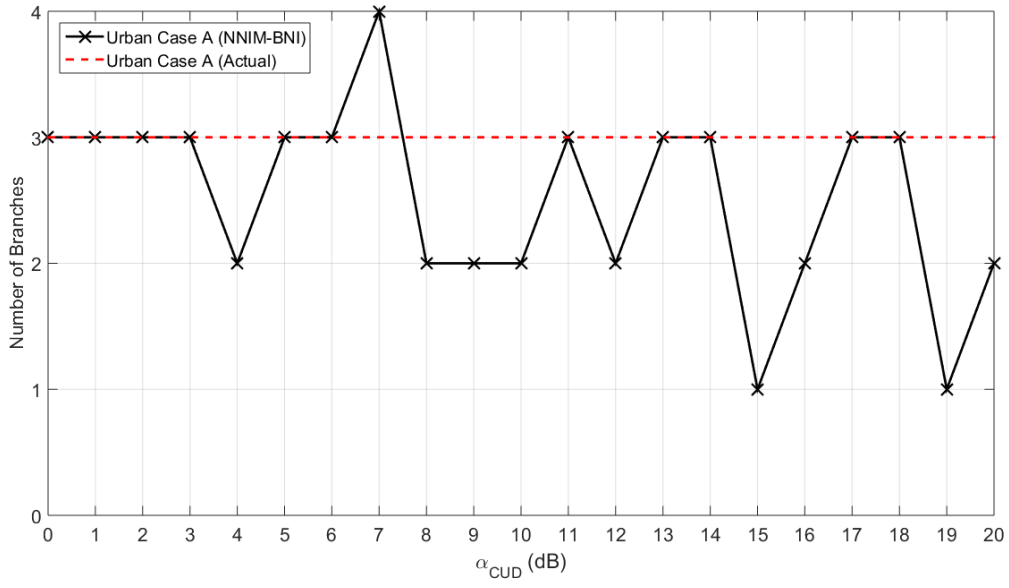
(a)
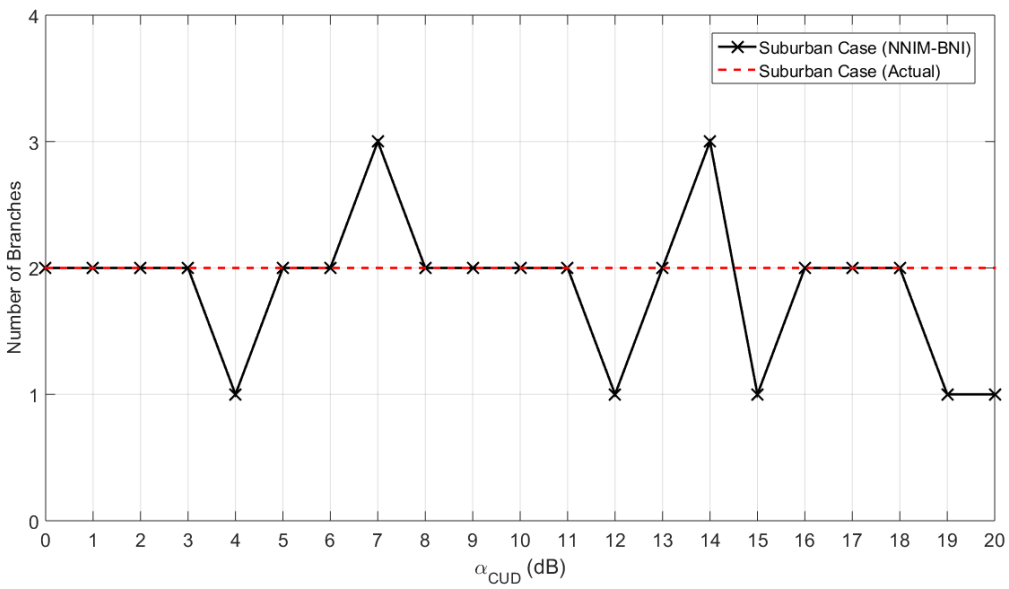
(b)
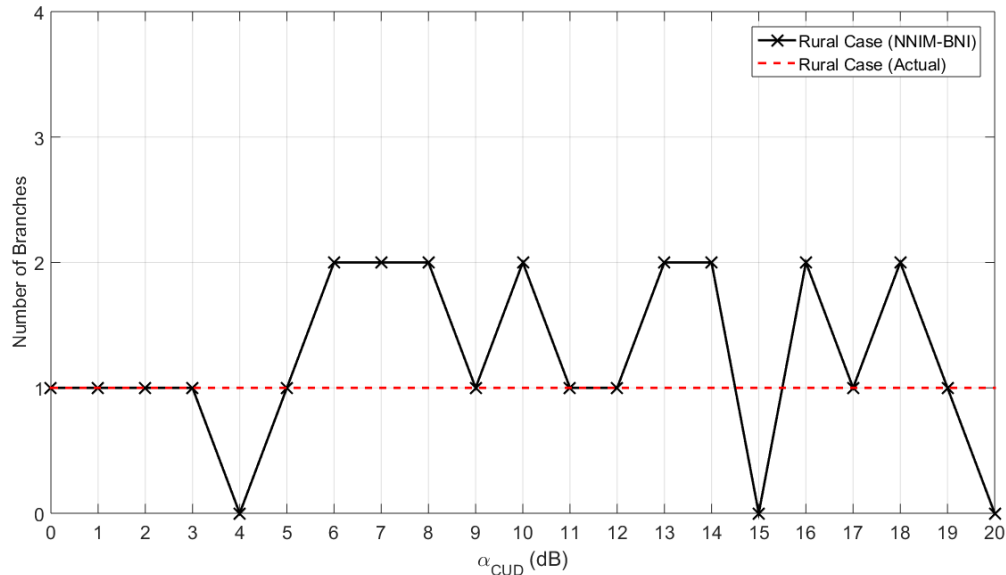
(c)

Figure 2. The rounded branch number approximations of NNIM-BNI with respect to a_{CUD} of CUD measurements. (a) Urban case A. (b) Suburban case. (c) Rural case.

From Table 3 and Figs. 2(a)-(c), several interesting remarks concerning the performance of NNIM-BNI can be pointed out when CUD measurement differences are superimposed. More specifically:

- As the RMSD results of the NNIM-BNI branch number approximation of the three indicative OV LV BPL topologies are examined, fluctuating RMSD values can be observed when the a_{CUD} of CUD measurements increases. In fact, the highest RMSD values of Table 3 that are equal to 0.99m and 0.96m are observed when a_{CUD} of CUD measurements is equal to 20dB and 19dB, respectively.
- When the a_{CUD} of CUD measurements increases the aforementioned RMSD behavior is reflected on Figs. 2(a)-(c); say, given the actual number of branches in each one of the three indicative OV LV BPL topologies, the rounded NNIM-BNI branch number approximation is almost equal to the actual number of branches for each one of the indicative OV LV BPL topologies when the a_{CUD} of CUD measurements remains lower or equal to 5dB. When a_{CUD} of CUD measurements becomes greater than 5dB, fluctuations of the rounded NNIM-BNI branch number approximations are observed in all the indicative OV LV BPL topologies. The highest deviations between the actual numbers of branches and the rounded NNIM-BNI branch number approximations, which are equal to 2 branches, is observed in the urban case A of Fig. 2(a) when a_{CUD} of CUD measurements is equal to 15dB and 19dB.

When a_{CUD} of CUD measurements remains low (i.e., below 5dB), NNIM-BNI can intrinsically mitigate measurement differences thus giving accurate rounded NNIM-BNI branch number approximations in the majority of the cases examined. Conversely, higher a_{CUD} values imply that appropriate mitigation techniques for the measurement differences should be externally applied to the measured coupling scheme transfer functions of eq.(3) prior to its consideration by NNIM-BNI.

3.2 NNIM-LLA – Base Scenario and Measurement Differences

As the base scenario of the operation of NNIM-LLA is concerned, the default operation settings B of Sec. 2.3 are assumed. Already been mentioned, the number of branches for the OV LV BPL topologies of the TIM OV LV BPL topology database are going to range from 0 (say, "LOS" case) up to 2 branches in this paper so as to allow the application of the default operation settings C bypassing: (i) the extremely high preparation time delay of the TIM OV LV BPL topology database when 3 branches need to be examined; and (ii) the high execution time of the MATLAB NN program of [47], [48] due to the high number of OV LV BPL topologies and the mechanism of avoiding the unacceptable NNIM-LLA approximations. Note that the suburban case, rural case and LOS case will be included into the TIM OV LV BPL topology database in contrast with [2] while only the distribution line and branch line lengths of the suburban case and rural case are going to be approximated by NNIM-LLA.

As the base scenario without measurement differences is concerned, the length approximations of the distribution and branch lines of NNIM-LLA are reported in Table 4 when the default operation settings B are assumed and the suburban case of Table 1 is examined. Apart from the original approximations that are given in black font color, the symmetrical approximations of NNIM-LLA for the suburban case are also given in blue font color. Similarly to [2] and for comparison reasons, the real lengths of the distribution and branch lines of the suburban case are presented while the RMSDs of NNIM-LLA approximations for the suburban case are also computed. Similarly to [1], [2], three executions of NNIM-LLA are reported for the suburban case per hidden layer. Table 5 is the same with Table 4 but for the rural case of Table 1. Similarly to [2], note that RMSD is computed in Tables 4 and 5 when 4 distribution line segments and 3 branches are assumed for the two examined indicative OV LV BPL topologies so that the RMSD effect of the inclusion of the two indicative OV LV BPL topologies during the preparation of the TIM OV LV BPL topology database can be assessed through the comparison of RMSD values with the respective ones of [2] where the two examined indicative OV LV BPL topologies are excluded from the TIM OV LV BPL topology database.

Table 4
Distribution and Branch Line Length Approximations of NNIM-LLA for the Suburban Case and Default Operation Settings B with no measurement differences (the symmetrical approximations are reported in blue font color and the suburban case is included in the TIM OV LV BPL topology database)

Indicative OV LV BPL Topologies of Table 1		Suburban case	RMSD	Notes
Distribution Line Length L $=[L_1 \quad L_2 \quad L_3 \quad 0]$ **Branch Line Length L**$_b$ $=[L_{b1} \quad L_{b2} \quad 0]$		[500m 400m 100m 0m] [50m 10m 0m]	-	-
NNIM-LLA **Approximated Distribution Line Length L**$_{NNIM-LLA}$ = $[L_{1,NNIM-LLA} \quad L_{2,NNIM-LLA} \quad L_{3,NNIM-LLA} \quad 0]$ **Approximated Branch Line Length L**$_{b,NNIM-LLA}$ = $[L_{b1,NNIM-LLA} \quad L_{b2,NNIM-LLA} \quad 0]$	1st execution	[61.95m 689.88m 248.17m 0m] [134.76m 158.64m 0m] [248.17m 689.88m 61.95m 0m] [158.64m 134.76m 0m]	216.18m 158.68m	Default Operation Settings B + 1 hidden layer
	2nd execution	[102.86m 509.38m 387.76m 0m] [143.86m 156.92m 0m] [387.76m 509.38m 102.86m 0m] [156.92m 143.86m 0m]	201.03m 87.77m	
	3rd execution	[106.12m 518.35m 375.53m 0m] [147.26m 162.89m 0m] [375.53m 518.35m 106.12m 0m] [162.89m 147.26m 0m]	199.25m 93.44m	
	1st execution	[109.41m 550.49m 340.10m 0m] [52.35m 48.63m 0m] [340.10m 550.49m 109.41m 0m] [48.63m 52.35m 0m]	182.97m 84.60m	Default Operation Settings B + 2 hidden layers
	2nd execution	[108.39m 532.83m 358.78m 0m] [228.83m 252.06m 0m] [358.78m 532.83m 108.39m 0m] [252.06m 228.8m 0m]	216.65m 134.36m	
	3rd execution	[57.82m 726.80m 216.30m 0m] [92.06m 94.40m 0m] [216.30m 726.80m 57.82m 0m] [94.40m 92.06m 0m]	215.39m 168.09m	
	1st execution	[113.61m 522.69m 363.59m 0m] [18.35m 4.77m 0m] [363.59m 522.69m 113.61m 0m] [4.77m 18.35m 0m]	183.17m 71.68m	Default Operation Settings B + 3 hidden layers
	2nd execution	[136.05m 516.21m 347.74m 0m] [19.02m 18.74m 0m] [347.74m 516.21m 136.05m 0m] [18.74m 19.02m 0m]	172.54m 74.68m	
	3rd execution	[99.88m 498.15m 402.01m 0m] [105.41m 149.07m 0m] [402.01m 498.15m 99.88m 0m] [149.07m 105.41m 0m]	201.19m 73.83m	
	1st execution	[207.41m 487.87m 305.00m 0m] [117.01m 143.02m 0m] [305.00m 487.87m 207.41m 0m]	150.02m	Default Operation Settings B

		[143.02m 117.01m 0m]	105.15m	+
	2nd execution	[138.22m 515.74m 346.14m 0m] [41.75m 40.02m 0m]	171.48m	4 hidden layers
		[346.14m 515.74m 138.22m 0m] [40.02m 41.75m 0m]	75.25m	
	3rd execution	[100.93m 573.22m 329.81m 0m] [25.96m 22.40m 0m]	186.24m	
		[329.81m 573.22m 100.93m 0m] [22.40m 25.96m 0m]	92.57m	
	1st execution	[106.50m 527.93m 365.66m 0m] [227.01m 217.69m 0m]	212.55m	Default Operation Settings B
		[365.66m 527.93m 106.50m 0m] [217.69m 227.01m 0m]	125.17m	+
	2nd execution	[152.23m 505.47m 313.49m 0m] [15.87m 20.17m 0m]	159.87m	5 hidden layers
		[313.49m 505.47m 152.23m 0m] [20.17m 15.87m 0m]	84.14m	
	3rd execution	[103.04m 522.04m 377.05m 0m] [43.48m 47.36m 0m]	189.23m	
		[377.05m 522.04m 103.04m 0m] [47.36m 43.48m 0m]	66.70m	

Table 5

Distribution and Branch Line Length Approximations of NNIM-LLA for the Rural Case and Default Operation Settings B with no measurement differences (the symmetrical approximations are reported in blue font color and the rural case is included in the TIM OV LV BPL topology database)

Indicative OV LV BPL Topologies of Table 1			**Rural case**	**RMSD**	**Notes**
Distribution Line Length L $=[L_1 \quad L_2 \quad 0 \quad 0]$ **Branch Line Length L$_b$** $=[L_{b1} \quad 0 \quad 0]$			[600m 400m 0m 0m] [300m 0m 0m]	-	-
NNIM-LLA **Approximated Distribution Line Length L$_{NNIM-LLA}$** $=$ $[L_{1,NNIM-LLA} \quad L_{2,NNIM-LLA} \quad 0 \quad 0]$ **Approximated Branch Line Length L$_{b,NNIM-LLA}$** $=$ $[L_{b1,NNIM-LLA} \quad 0 \quad 0]$	1st execution		[278.75m 770.31m 0m 0m] [232.13m 0m 0m]	187.06m	Default Operation Settings B
			[770.31m 278.75m 0m 0m] [232.13m 0m 0m]	83.08m	+
	2nd execution		[205.33m 796.69m 0m 0m] [164.04m 0m 0m]	217.65m	1 hidden layer
			[796.69m 205.33m 0m 0m] [164.04m 0m 0m]	116.54m	
	3rd execution		[280.44m 719.56m 0m 0m] [299.50m 0m 0m]	170.81m	
			[719.56m 280.44m 0m 0m] [299.50m 0m 0m]	63.91m	
	1st execution		[266.99m 733.42m 0m 0m] [215.69m 0m 0m]	180.94m	Default Operation Settings B
			[733.42m 266.99m 0m 0m] [215.69m 0m 0m]	78.01m	+

2nd execution	[297.29m 700.86m 0m 0m] [276.04m 0m 0m]	161.57m	2 hidden layers
	[700.86 297.29m 0m 0m] [276.04m 0m 0m]	55.16m	
3nd execution	[308.12m 692.59m 0m 0m] [278.26m 0m 0m]	156.42m	
	[692.59m 308.12m 0m 0m] [278.26m 0m 0m]	49.98m	
1st execution	[278.28m 631.75m 0m 0m] [112.72m 0m 0m]	165.74m	Default Operation Settings B + 3 hidden layers
	[631.75 278.28m 0m 0m] [112.72m 0m 0m]	85.27m	
2nd execution	[239.99m 760.01m 0m 0m] [299.979397173821m 0m 0m]	192.43m	
	[760.01m 239.99m 0m 0m] [299.97m 0m 0m]	85.53m	
3nd execution	[296.21m 731.66m 0m 0m] [210.946885278590m 0m 0m]	173.30m	
	[731.66m 296.21m 0m 0m] [210.95m 0m 0m]	71.75m	
1st execution	[250.02m 749.98m 0m 0m] [300.00m 0m 0m]	187.07m	Default Operation Settings B + 4 hidden layers
	[749.98m 250.02m 0m 0m] [300.00m 0m 0m]	80.17m	
2nd execution	[350.10m 649.68m 0m 0m] [295.77m 0m 0m]	133.53m	
	[649.68m 350.10m 0m 0m] [295.77m 0m 0m]	26.66m	
3nd execution	[349.94m 628.11m 0m 0m] [275.66m 0m 0m]	128.26m	
	[628.11m 349.94m 0m 0m] [275.66m 0m 0m]	23.57m	
1st execution	[234.69m 781.13m 0m 0m] [325.14m 0m 0m]	199.77m	Default Operation Settings B + 5 hidden layers
	[781.13m 234.69m 0m 0m] [325.14m 0m 0m]	93.17m	
2nd execution	[349.82m 649.66m 0m 0m] [300.21m 0m 0m]	133.59m	
	[649.66m 349.82m 0m 0m] [300.21m 0m 0m]	26.68m	
3nd execution	[299.03m 686.21m 0m 0m] [310.08m 0m 0m]	157.03m	
	[686.21m 299.03m 0m 0m] [310.08m 0m 0m]	50.33m	

By comparing Tables 4 and 5 with the respective Tables 3 and 4 of [2], it is evident that the inclusion of the examined indicative OV LV BPL topologies in the TIM OV LV BPL topology database affects the accuracy of NNIM-LLA. Also, the mechanism for encountering the unacceptable NNIM-LLA approximations fills the missing approximations in Tables 4 and 5, especially those when the high number of hidden layers is assumed. In total, apart from the elimination of the unacceptable NNIM-LLA approximations, the RMSD values get significantly improved regardless of the examined indicative OV LV BPL topology and the number of the applied hidden layers. To graphically validate the aforementioned RMSD improvement, the best RMSD values of the NNIM-LLA approximations (say, the minimum RMSD value between the original and symmetrical approximated OV LV BPL topology given the number of execution and the number of hidden layers) of Table 4 are plotted in Fig. 3(a) with respect to the number of hidden layers when the default operation settings B are assumed. In Fig. 3(b), the same plot with Fig. 3(a) is presented but for the rural case of Table 5.

(a)

(b)
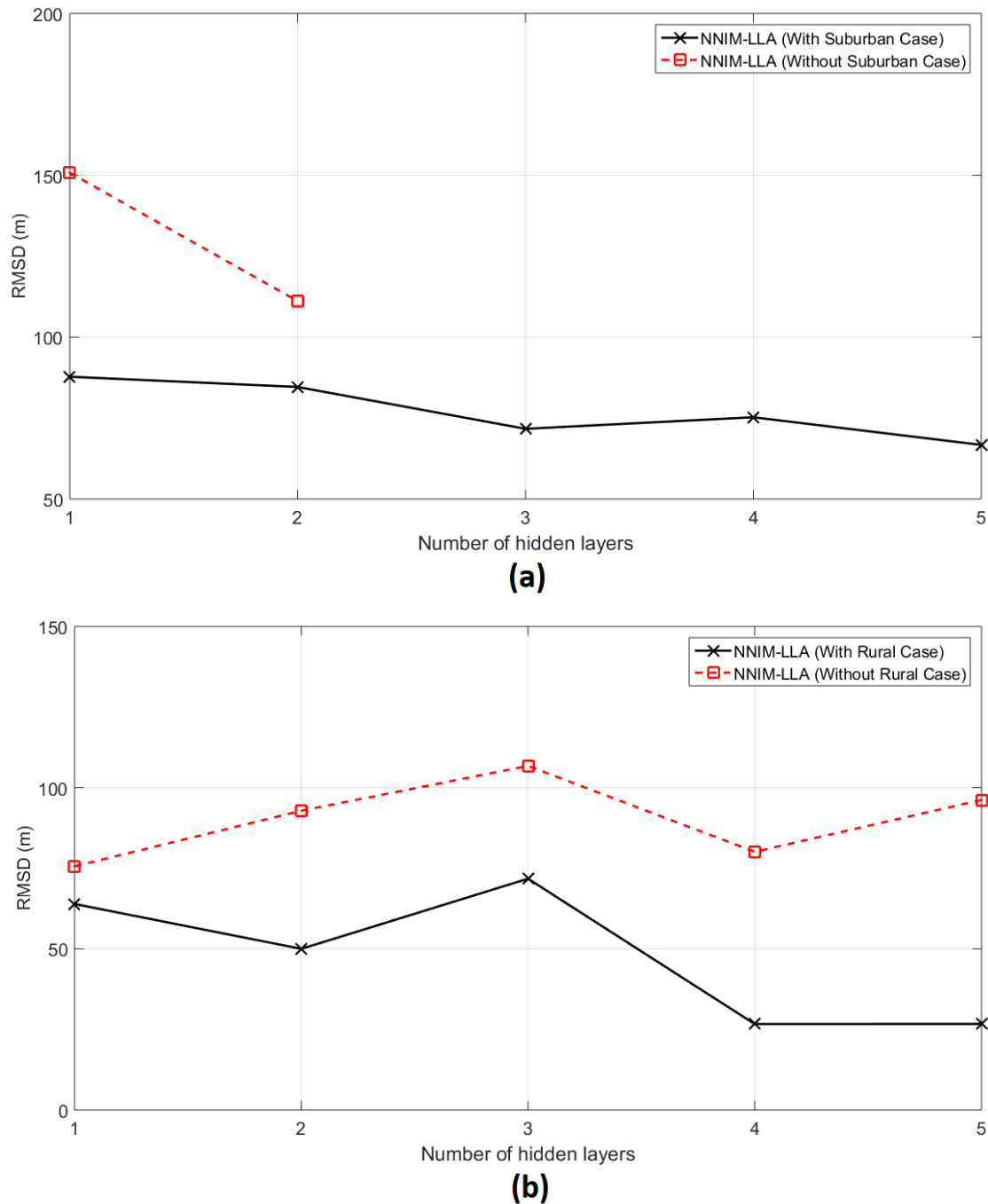
Figure 3. Best RMSD values of NNIM-BNI approximations whether the examined indicative OV LV BPL topology is included in the preparation of the TIM OV LV BPL topology database or not. (a) Suburban case. (b) Rural case.

Already been observed in Tables 3-5, the inclusion of the indicative OV LV BPL topologies in the TIM OV LV BPL topology database and the mechanism for preventing unacceptable approximations significantly improve the performance and accuracy of NN related approximations of this paper, say, NNIM-BNI and NNIM-LLA. Also, the following assumptions are made for the following CUD measurement study during the application of NNIM-LLA, namely:

- The best RMSD values of NNIM-BNI approximations imply that the selection between the original and symmetrical approximations can be fulfilled. Anyway, in accordance with [2], additional topological pieces of information or empirical observations so that the distinction between these approximated OV LV BPL topologies may help towards the selection between the original and symmetrical approximations.

- Similarly to Sec.3.1 and without affecting the generality of the analysis, only one repetition and two hidden layers are going to be applied in the following CUD measurement analysis. As the one repetition is considered, best RMSD values of Tables 4 and 5 can be considered to be relatively close for the different repetitions for given examined indicative OV LV BPL topology and number of hidden layers. As two hidden layers are assumed, best RMSD values of Figs. 3(a) and 3(b) can be considered to be relatively close for the different numbers of hidden layers for given examined indicative OV LV BPL topology. Anyway, only one hidden layer is assumed to be sufficient in general, but one and five hidden layers are assumed so that the NNIM-LLA performance against the measurement differences and the total duration time for the different default operation settings can be investigated in the rest of this paper.

As the impact of CUD measurement differences on the performance of NNIM-LLA is investigated, similarly to Table 4, in Table 6, given the amplitudes of coupling scheme channel transfer functions contaminated with measurements in dB for the suburban case of Table 1, NNIM-LLA gives as output its respective approximations of the distribution and branch line lengths when various a_{CUD} values of CUD measurements are assumed. Note that one $1 \times Q = 1 \times (88 - 3) = 1 \times 85$ measurement difference line vector for each a_{CUD} value that ranges from 0dB to 20dB is superimposed to the amplitudes of the coupling scheme channel transfer functions of the suburban case for the respective NNIM-LLA approximation cases. Also, the best RMSD value between the approximated original and symmetrical OV LV topologies and the respective OV LV BPL topology are presented per a_{CUD} in Table 6. Table 7 is similar to Table 6 but for the rural case of Table 1. Note that the same 21×85 measurement difference vector with Table 6 is here superimposed to the amplitudes of the coupling scheme channel transfer functions of the rural case for all the examined NNIM-LLA approximation cases. In Tables 6 and 7, the default operation settings B of Sec.2.3 are applied when one hidden layer is assumed during the NNIM-LLA simulations.

Table 6
Distribution and Branch Line Length Approximations of NNIM-LLA for the Suburban Case and Default Operation Settings B for Different a_{CUD} Values of CUD Measurements (the symmetrical approximations are reported in blue font color and the suburban case is included in the TIM OV LV BPL topology database)

Indicative OV LV BPL Topologies of Table 1		Suburban Case	RMSD	Notes
Distribution Line Length L =$[L_1 \quad L_2 \quad L_3 \quad 0]$ **Branch Line Length L_b** =$[L_{b1} \quad L_{b2} \quad 0]$		[500m 400m 100m 0m] [50m 10m 0m]	-	-
NNIM-LLA **Approximated Distribution Line Length** $L_{NNIM-LLA}$ = $[L_{1,NNIM-LLA} \quad L_{2,NNIM-LLA} \quad L_{3,NNIM-LLA} \quad 0]$ **Approximated Branch Line Length** $L_{b,NNIM-LLA}$ = $[L_{b1,NNIM-LLA} \quad L_{b2,NNIM-LLA} \quad 0]$	a_{CUD} **of CUD Measurements (dB)**			Default Operation Settings B + 1 hidden layer
	0	[514.49m 335.46m 150.05m 0m] [119.28m 106.45m 0m]	54.75m	
	1	[225.07m 718.12m 56.81m 0m] [168.35m 152.43m 0m]	174.42m	
	2	[263.82m 653.95m 82.22m 0m] [81.64m 75.23m 0m]	134.08m	
	3	[511.72m 343.71m 144.57m 0m] [161.23m 157.85m 0m]	75.14m	
	4	[221.28m 716.98m 61.75m 0m] [162.76m 139.54m 0m]	172.84m	
	5	[238.17m 707.35m 54.49m 0m] [174.80m 150.64m 0m]	169.22m	
	6	[229.59m 711.73m 58.68m 0m] [158.89m 141.56m 0m]	169.53m	
	7	[752.89m 34.22m 212.89m 0m] [147.32m 142.86m 0m]	184.24m	
	8	[513.37m 380.09m 131.32m 0m] [182.12m 137.55m 0m]	71.00m	
	9	[154.58m 805.21m 40.18m 0m] [152.33m 138.91m 0m]	211.85m	
	10	[210.15m 723.15m 66.70m 0m] [156.13m 146.19m 0m]	177.02m	
	11	[239.26m 694.45m 66.28m 0m] [162.12m 155.94m 0m]	164.62m	
	12	[214.29m 732.38m 53.34m 0m] [153.16m 141.86m 0m]	178.21m	
	13	[739.43m 47.12m 213.45m 0m] [155.50m 149.49m 0m]	179.41m	
	14	[756.80m 28.69m 214.51m 0m] [147.00m 146.54m 0m]	187.07m	
	15	[232.00m 716.22m 51.77m 0m] [169.73m 155.13m 0m]	173.01m	
	16	[231.56m 704.34m 64.10m 0m] [166.45m 147.98m 0m]	168.42m	
	17	[734.08m 66.52m 199.40m 0m] [146.32m 139.96m 0m]	169.89m	
	18	[709.93m 87.39m 202.67m 0m] [155.54m 158.97m 0m]	162.86m	
	19	[217.50m 713.43m 69.07m 0m] [162.53m 144.14m 0m]	173.06m	

| | 20 | [219.18m 708.39m 72.43m 0m] [162.78m 132.21m 0m] | 170.03m | |

Table 7
Distribution and Branch Line Length Approximations of NNIM-LLA for the Rural Case and Default Operation Settings B for Different a_{CUD} Values of CUD Measurements (the symmetrical approximations are reported in blue font color and the rural case is included in the TIM OV LV BPL topology database)

Indicative OV LV BPL Topologies of Table 1		**Rural Case**	**RMSD**	**Notes**
Distribution Line Length L $=[L_1 \quad L_2 \quad 0 \quad 0]$		[600m 400m 0m 0m]	-	-
Branch Line Length L$_b$ $=[L_{b1} \quad 0 \quad 0]$		[300m 0m 0m]		
NNIM-LLA **Approximated Distribution Line Length** $L_{NNIM-LLA} = [L_{1,NNIM-LLA} \quad L_{2,NNIM-LLA} \quad 0 \quad 0]$ **Approximated Branch Line Length** $L_{b,NNIM-LLA} = [L_{b1,NNIM-LLA} \quad 0 \quad 0]$	$\boldsymbol{a_{CUD}}$ **of CUD Measurements (dB)**			Default Operation Settings B + 1 hidden layer
	0	[591.84m 410.07m 0m 0m] [39.52m 0m 0m]	98.58m	
	1	[785.00m 216.36m 0m 0m] [204.93m 0m 0m]	104.87m	
	2	[839.77m 207.39m 0m 0m] [329.55m 0m 0m]	116.78m	
	3	[804.46m 108.34m 0m 0m] [75.35m 0m 0m]	159.17m	
	4	[890.85m 109.17m 0m 0m] [7.61m 0m 0m]	190.74m	
	5	[701.77m 421.63m 0m 0m] [250.88m 0m 0m]	43.49m	
	6	[740.00m 260.00m 0m 0m] [0m 0m 0m]	135.86m	
	7	[734.26m 223.51m 0m 0m] [101.29m 0m 0m]	112.54m	
	8	[983.99m 23.43m 0m 0m] [218.82m 0m 0m]	205.58m	
	9	[745.74m 241.63m 0m 0m] [189.25m 0m 0m]	91.49m	
	10	[787.87m 212.13m 0m 0m] [151.87m 0m 0m]	114.97m	
	11	[660.41m 338.10m 0m 0m] [202.32m 0m 0m]	49.31m	
	12	[765.06m 238.30m 0m 0m] [160.25m 0m 0m]	102.07m	
	13	[665.00 474.69 0m 0m] [257.86m 0m 0m]	40.67m	
	14	[573.36m 426.64m 0m 0m] [328.51m 0m 0m]	17.86m	
	15	[737.08m 114.20m 0m 0m] [197.60m 0m 0m]	125.90m	
	16	[590.81m 196.27m 0m 0m] [144.09m 0m 0m]	97.03m	
	17	[722.22m 277.78m 0m 0m] [144.45m 0m 0m]	87.89m	

18	[750.02m 249.98m 0m 0m] [162.60m 0m 0m]	95.54m	
19	[641.08m 353.70m 0m 0m] [242.41m 0m 0m]	31.96m	
20	[605.22m 309.40m 0m 0m] [368.12m 0m 0m]	42.89m	

From Tables 6 and 7, NNIM-LLA presents a similar behavior with NNIM-BNI concerning the intrinsic mitigation of the measurement differences; although measurement differences affect RMSD values of the NNIM-LLA approximations, a strong correlation between RMSD values and a_{CUD} values of CUD measurements is not observed in the examined suburban and rural cases. Similarly to Table 3 and Figs. 2(a)-(c), a highly fluctuating RMSD trend can be observed when the a_{CUD} of CUD measurements increases in suburban and rural cases. Indeed, with reference to Table 4, the maximum difference between the best RMSD values of the three executions is equal to 70.91m for the suburban case when one hidden layer is assumed (i.e. RMSD of the 1st execution minus the RMSD of the 3nd execution). With reference to Table 6, the maximum RMSD difference between the best values of the 21 different measurement difference cases is equal to 157.10m for the suburban case when one hidden layer is again assumed (i.e. RMSD of the measurement difference case of a_{CUD}=9dB minus the RMSD of the measurement difference case of a_{CUD}=0dB). As the rural case is concerned, the aforementioned maximum differences are equal to 52.63m and 187.72m with reference to Tables 5 and 7, respectively. Therefore, a successful mitigation technique against the measurement differences should be benchmarked through the prism of its performance to reduce the maximum difference between the best values of the 21 different measurement difference cases thus stabilizing the fluctuating behavior of the RMSD values of the NNIM-LLA approximations. Finally, for comparison reasons, the total duration time for preparing both Tables 6 and 7 is equal to 3,505s for the default operation settings B and 21 different measurement difference cases when one hidden layer is assumed. For the time computations of this paper, the used PC consists of an 1.86GHz Intel Pentium with 4GB RAM while the worst case scenario of the preparation of TIM OV LV BPL topology database is applied where the appropriate TIM OV LV BPL topology is prepared per indicative OV LV BPL topology and CUD measurement difference case in compliance with the database representativeness, which is analyzed in [2] for the operation of NNIM-LLA and mentioned in Sec.2.3.

3.3 NNIM-LLA – Default Operation Settings against Measurement Differences

In accordance with [1], the accuracy degree of the TIM OV LV BPL topology database, which is affected by the selection of the applied default operation settings, has significantly improved RMSDs of the branch number approximations of NNIM-BNI. In this paper, default operation settings C, which allow higher accuracy degree of the TIM OV LV BPL topology database in comparison with the one of default operation settings B, are applied in order to improve the performance of NNIM-LLA against the measurement differences. But the higher accuracy degree of the TIM OV LV BPL topology requires higher time duration times of NNIM-LLA that can be a prohibitive task when the required accuracy is set to be very high.

Similarly to Tables 6 and 7, in Table 8, NNIM-LLA gives approximations of the distribution and branch line lengths when the same a_{CUD} values of CUD measurements of

Table 6 are applied given the amplitudes of coupling scheme channel transfer functions contaminated with measurements in dB for the suburban case of Table 1. The same 21×85 measurement difference vector with Tables 6 and 7 is here superimposed to the amplitudes of the coupling scheme channel transfer functions of the suburban case for all the 21 NNIM-LLA approximation cases. Similarly to Table 6, the best RMSD value between the approximated original and symmetrical OV LV topologies and the respective OV LV BPL topology are presented per a_{CUD} value in Table 8. Conversely to Table 6, the default operation settings C are adopted during the preparation of Table 8 instead of the default operation settings B. Table 9 is similar to Table 8 but for the rural case of Table 7. To graphically examine the impact of the default operation settings that support a more elaborate version of the TIM OV LV BPL topology database on the mitigation of the measurement differences, the best RMSD values of the NNIM-LLA approximations (say, the minimum RMSD value between the original and symmetrical approximated OV LV BPL topology given the execution and the number of hidden layers) of Tables 6 and 8 are plotted in Fig. 4(a) with respect to the a_{CUD} of the applied CUD measurements when the default operation settings B and C are assumed, respectively. In Fig. 4(b), the same plot with Fig. 4(a) is given but for the rural case and with respect to Tables 7 and 9.

Table 8
Distribution and Branch Line Length Approximations of NNIM-LLA for the Suburban Case and Default Operation Settings C for Different a_{CUD} Values of CUD Measurements (the symmetrical approximations are reported in blue font color and the suburban case is included in the TIM OV LV BPL topology database)

Indicative OV LV BPL Topologies of Table 1		Suburban Case	RMSD	Notes
Distribution Line Length L $=[L_1 \quad L_2 \quad L_3 \quad 0]$ **Branch Line Length L$_b$** $=[L_{b1} \quad L_{b2} \quad 0]$		[500m 400m 100m 0m] [50m 10m 0m]	-	-
NNIM-LLA **Approximated Distribution Line Length** $\mathbf{L_{NNIM-LLA}} =$ $[L_{1,NNIM-LLA} \quad L_{2,NNIM-LLA} \quad L_{3,NNIM-LLA} \quad 0]$ **Approximated Branch Line Length** $\mathbf{L_{b,NNIM-LLA}} =$ $[L_{b1,NNIM-LLA} \quad L_{b2,NNIM-LLA} \quad 0]$	a_{CUD} **of CUD Measurements (dB)**			Default Operation Settings C + 1 hidden layer
	0	[715.32m 71.28m 213.39m 0m] [151.51m 147.17m 0m]	167.50m	
	1	[284.39m 650.09m 65.52m 0m] [156.12m 143.70m 0m]	141.10m	
	2	[687.71m 110.29m 202.00m 0m] [149.84m 144.56m 0m]	150.07m	
	3	[724.46m 62.99m 212.54m 0m] [151.86m 145.33m 0m]	171.26m	
	4	[716.60m 72.80m 210.60m 0m] [153.16m 143.41m 0m]	166.75m	
	5	[282.40m 656.36m 61.24m 0m] [154.76m 149.40m 0m]	143.91m	
	6	[706.15m 81.71m 212.15m 0m] [152.85m 144.42m 0m]	162.58m	
	7	[265.15m 676.45m 58.40m 0m] [157.69m 150.64m 0m]	153.38m	
	8	[720.49m 70.19m 209.32m 0m] [153.10m 144.78m 0m]	168.24m	
	9	[720.59m 67.92m 211.48m 0m] [152.64m 144.57m 0m]	169.03m	

	10	[280.41m 654.99m 64.61m 0m] [156.07m 148.88m 0m]	143.94m
	11	[283.95m 649.47m 66.58m 0m] [152.87m 146.65m 0m]	141.06m
	12	[281.65m 659.43m 58.93m 0m] [154.30m 149.01m 0m]	144.85m
	13	[272.07m 670.23m 57.71m 0m] [156.43m 147.97m 0m]	149.82m
	14	[700.18m 93.36m 206.46m 0m] [155.07m 148.79m 0m]	158.45m
	15	[283.23m 653.08m 63.69m 0m] [155.45m 142.52m 0m]	141.94m
	16	[719.25m 67.76m 212.99m 0m] [151.70m 143.67m 0m]	168.79m
	17	[280.28m 652.45m 67.27m 0m] [156.30m 148.75m 0m]	143.24m
	18	[271.65m 670.15m 58.20m 0m] [151.95m 149.16m 0m]	149.58m
	19	[281.00m 654.80m 64.20m 0m] [155.11m 147.51m 0m]	143.49m
	20	[270.20m 672.51m 57.29m 0m] [154.15m 147.87m 0m]	150.60m

Table 9
Distribution and Branch Line Length Approximations of NNIM-LLA for the Rural Case and Default Operation Settings C for Different a_{CUD} Values of CUD Measurements (the symmetrical approximations are reported in blue font color and the rural case is included in the TIM OV LV BPL topology database)

Indicative OV LV BPL Topologies of Table 1		Rural Case	RMSD	Notes
Distribution Line Length L $=[L_1 \quad L_2 \quad 0 \quad 0]$ **Branch Line Length L**$_b$ $=[L_{b1} \quad 0 \quad 0]$		[600m 400m 0m 0m] [300m 0m 0m]	-	-
NNIM-LLA **Approximated Distribution Line Length** $L_{NNIM-LLA} = [L_{1,NNIM-LLA} \quad L_{2,NNIM-LLA} \quad 0 \quad 0]$ **Approximated Branch Line Length** $L_{b,NNIM-LLA} = [L_{b1,NNIM-LLA} \quad 0 \quad 0]$	a_{CUD} **of CUD Measurements (dB)**			Default Operation Settings C + 1 hidden layer
	0	[790.25m 189.38m 0m 0m] [202.45m 0m 0m]	113.44m	
	1	[750.59m 225.04m 0m 0m] [223.77m 0m 0m]	91.88m	
	2	[716.01m 283.97m 0m 0m] [191.34m 0m 0m]	74.38m	
	3	[732.49m 267.51m 0m 0m] [261.42m 0m 0m]	72.30m	
	4	[665.20m 334.66m 0m 0m] [11.30m 0m 0m]	114.56m	
	5	[740.38m 245.13m 0m 0m] [145.37m 0m 0m]	98.27m	
	6	[670.96m 329.03m 0m 0m] [126.16m 0m 0m]	75.87m	
	7	[739.60m 260.40m 0m 0m] [322.50m 0m 0m]	75.10m	

	8	[779.41m 220.59m 0m 0m] [121.76m 0m 0m]	117.20m	
	9	[620.96m 379.04m 0m 0m] [655.98m 0m 0m]	135.01m	
	10	[748.68m 251.30m 0m 0m] [94.85m 0m 0m]	111.04m	
	11	[833.91m 164.90m 0m 0m] [170.90m 0m 0m]	134.51m	
	12	[829.14m 166.38m 0m 0m] [142.01m 0m 0m]	137.34m	
	13	[776.44m 223.03m 0m 0m] [95.56m 0m 0m]	122.03m	
	14	[685.64m 93.61m 0m 0m] [50.95m 0m 0m]	152.71m	
	15	[730.21m 269.73m 0m 0m] [93.68m 0m 0m]	104.54m	
	16	[808.70m 313.49m 0m 0m] [94.36m 0m 0m]	115.47m	
	17	[751.79m 248.21m 0m 0m] [46.39m 0m 0m]	125.58m	
	18	[760.09m 235.28m 0m 0m] [95.14m 0m 0m]	116.33m	
	19	[691.35m 358.99m 0m 0m] [153.33m 0m 0m]	67.12m	
	20	[727.00m 202.77m 0m 0m] [165.94m 0m 0m]	102.12m	
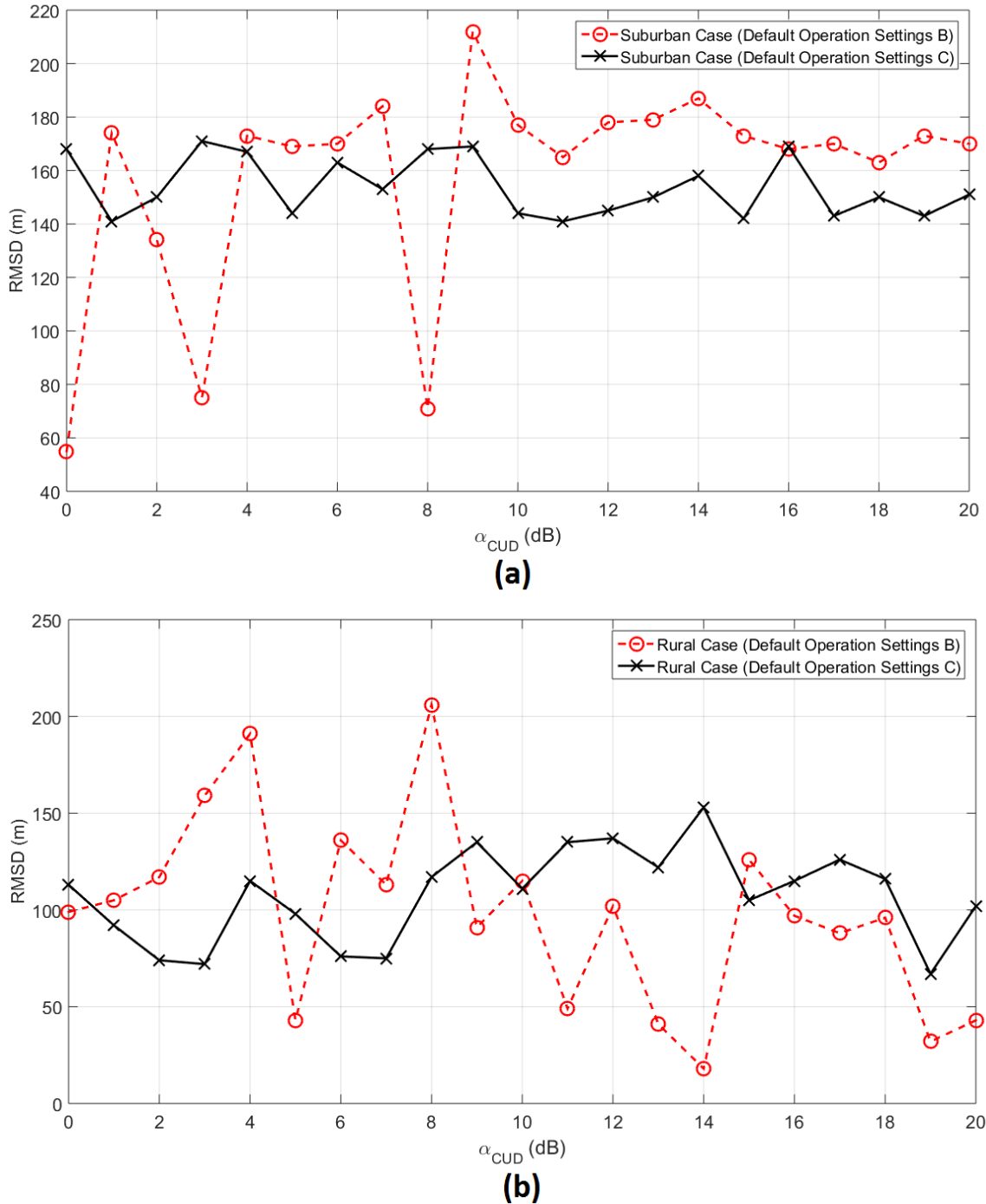
Figure 4. Best RMSD values of NNIM-LLA approximations with respect to a_{CUD} of the applied CUD measurements when the default operation settings B and C are applied and one hidden layer is assumed. (a) Suburban case. (b) Rural case.

Comparing Tables 8 and 9 and examining Figs. 4(a) and 4(b), it is obvious that the adoption of default operation settings that create more elaborate version of the TIM OV LV BPL topology database, such as the default operation settings C of this Section, reduces the mean RMSD of the NNIM-LLA approximations but the aforementioned reduction is constrained by the representativeness of the OV LV BPL topologies in the

TIM OV LV BPL topology databases that remains unaffected either in the suburban case or in rural one [1], [2]. In addition, the default operation settings C critically reduce the fluctuations of NNIM-LLA approximations with respect to a_{CUD} of the applied CUD measurements either in suburban case or in rural one; for the suburban case and with reference to Table 8, the maximum difference between the best values of the 21 different measurement difference cases gets improved from 157.10m to 30.20m when one hidden layer is assumed and the default operation settings B and C are applied, respectively. Similarly, for the rural case and with reference to Table 9, the maximum difference between the best values of the 21 different measurement difference cases gets improved from 187.72m to 85.59m when one hidden layer is assumed and the default operation settings B and C are applied, respectively. As already been mentioned, a trade-off between the improved performance of NNIM-LLA when more elaborate default operation settings are applied and the total duration time of NNIM-LLA simulation occurs; the total duration time for preparing both Tables 8 and 9 increases up to 29,364s in comparison with the total duration time of 3,505s for preparing both Tables 6 and 7.

To validate the beneficial role of the default operation settings C against the CUD measurement differences when various a_{CUD} are applied, the same procedure, which is followed in Table 8, Table 9 and Figure 4 for one hidden layer, is repeated when five hidden layers are applied during the NNIM-LLA approximations. Similarly to Fig. 4(a), the best RMSD values of the NNIM-LLA approximations for the suburban case are plotted in Fig. 5(a) with respect to the a_{CUD} of the applied CUD measurements when the default operation settings B and C are assumed, respectively, and five hidden layers are applied. In Fig. 5(b), the same plot with Fig. 5(a) is given but for the rural case. Note that the same 21×85 measurement difference vector, which is applied across the latter NNIM-LLA approximations, is again used for the NNIM-LLA approximation cases of Figs. 5(a) and 5(b). For the sake of the paper size reduction, the respective Tables to Tables 8 and 9 for preparing Figs. 5(a) and 5(b) are not analytically presented in this subsection.

(a)

(b)
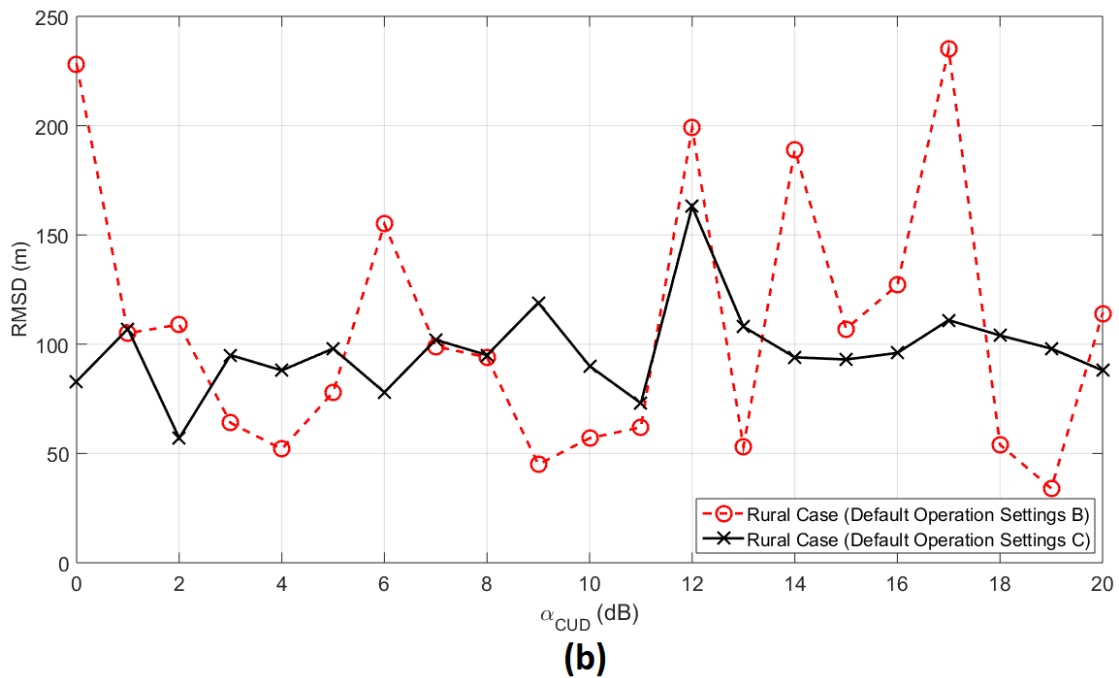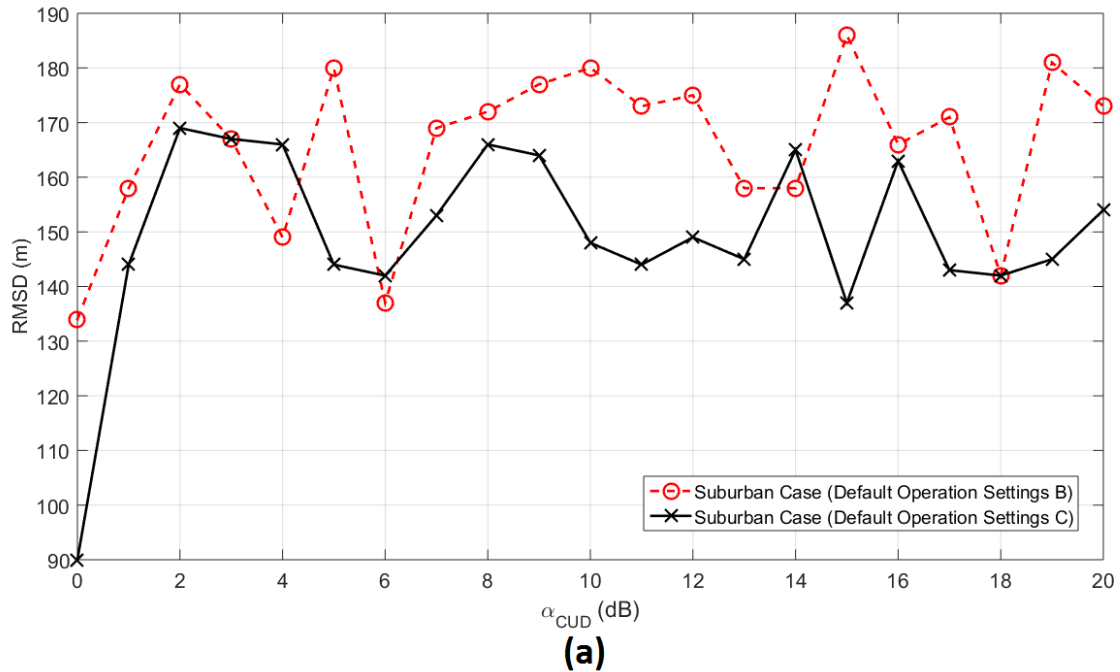
Figure 5. Best RMSD values of NNIM-LLA approximations with respect to a_{CUD} of the applied CUD measurements when the default operation settings B and C are applied and five hidden layers are assumed. (a) Suburban case. (b) Rural case.

Observing Figs. 5(a) and 5(b), the mitigation efficiency of the default operation settings C against CUD measurement differences is again validated in the suburban and rural cases, respectively, when five hidden layers are assumed. Apart from the similar RMSD general image and RMSD values of Figs. 5(a) and 5(b) with the respective Figs. 4(a) and 4(b), the application of the default operation settings C indeed reduces the mean

RMSD and the RMSD fluctuations when compared to the ones of the default operation settings B; for the suburban case of Fig. 5(a), the maximum difference between the best RMSD values of the 21 different measurement difference cases gets improved from 52m to 32m when five hidden layers are assumed and the default operation settings B and C are applied, respectively (note that the best RMSD value of default operation settings C when a_{CUD} is equal to 0dB is excluded during the previous maximum difference computation due to its extremeness). Similarly, for the rural case and with reference to Table 9, the maximum difference between the best values of the 21 different measurement difference cases gets improved from 201m to 106m when five hidden layers are assumed and the default operation settings B and C are applied, respectively. The trade-off between the improved performance of NNIM-LLA and the total time duration time of NNIM-LLA simulation also occurs; the total time duration time for the suburban and rural case plots of Figs. 5(a) and 5(b) when the default operation settings C are applied increases up to 45,556s in comparison with the total duration time of 11,270s for preparing the suburban and rural case plots of Figs. 5(a) and 5(b) when the default operation settings B have been applied. Note that the two improvements of Sec.2.3 that deal with the unacceptable NNIM-LLA approximations of [2] have achieved the elimination of the unacceptable NNIM-LLA approximations in Figs. 5(a) and 5(b) but the increased total duration times of Figs. 5(a) and 5(b) with comparison to the ones of Figs. 4(a) and 4(b) are explained by the fact that the latter total time duration times also include the required repetitions of the MATLAB NN program of [47], [48] that programmatically supports the NNIM-LLA approximations so that the unacceptable NNIM-LLA approximations can be eliminated. Surely, the worst case scenario of the preparation of TIM OV LV BPL topology database per indicative OV LV BPL topology and CUD measurement difference case significantly deteriorates the aforementioned total time duration times thus indicating the significant delays that may be present if more elaborate restrictions concerning the possible database representativeness improvements that may be applied during the preparation of TIM OV LV BPL topology database per examined case. This clearly unveils the need for: (i) smarter countermeasure techniques against measurement differences prior to the application of the MATLAB NN program of NNIM-LLA; and (ii) tailored-made and representative segments of the TIM OV LV BPL database that holds per case groups and not per examined case.

After the previous observations, the companion paper of [52] starts the challenge of searching and adopting of appropriate countermeasure techniques against measurement differences from the literature so that the performance of NNIM-LLA could be improved in terms of their RMSD fluctuations and, at the same time, the mean RMSD gets improved and the total duration time remains close to the total duration time of the default operation setting basis. From the literature, the application of piecewise monotonic data approximation methods, such as L1PMA, L2WPMA and L2CXCV which have theoretically been presented and experimentally verified in [30], [53]-[59] as output module, is assessed as the intermediate module after the DHM module and before the NNIM-LLA module when CUD measurement differences of various a_{CUD} values occur during the operation of the OV LV BPL networks.

5. Conclusions

In this paper, the impact of CUD measurement differences on the performance of NNIM-BNI and NNIM-LLA has been assessed as well as the countermeasure role of the adoption of diverse default operation settings against measurement differences. First, the effect of the presence of CUD measurement differences of various a_{CUD} values has been examined. Both NN methodologies have presented a strong inherent mitigation efficiency against CUD measurement differences and especially those of low a_{CUD} values (i.e., a_{CUD} values lower than approximately 5dB). CUD measurement differences of high a_{CUD} values primarily affect the stability of the NNIM-BNI and NNIM-LLA approximations in terms of their RMSD fluctuations rather than mean RMSD that depends on the accuracy of the applied TIM OV LV BPL topology database and its representativeness. Second, the adoption of default operation settings that allows more elaborate versions of the applied TIM OV LV BPL topology significantly improves the stability of the approximations by reducing the RMSD approximation fluctuations. Hence, the adoption of the aforementioned default operation settings can act as a countermeasure technique in environments where unknown or high CUD measurement differences are observed. However, a trade-off between the accuracy of the applied default operation settings and the total duration time of NNIM-LLA has been revealed. Third, improvements for the finer operation of NN identification methodologies have been examined, such as the BPL topology database representativeness, the BPL topology inclusion into the BPL topology database and the unacceptable approximation elimination technique. The application of more elaborate countermeasure techniques against measurement differences and / or representative segments of the TIM OV LV BPL database should be further investigated so that more accurate and stable NNIM-BNI and NNIM-LLA approximations can occur.

CONFLICTS OF INTEREST

The authors declare that there is no conflict of interests regarding the publication of this paper.

References

[1]   Lazaropoulos, A. G. (2021). Information Technology, Artificial Intelligence and Machine Learning in Smart Grid – Performance Comparison between Topology Identification Methodology and Neural Network Identification Methodology for the Branch Number Approximation of Overhead Low-Voltage Broadband over Power Lines Network Topologies. *Trends in Renewable Energy, 7*, 87-113. doi: https://doi.org/10.17737/tre.2021.7.1.00133

[2]   Lazaropoulos, A. G., & Leligou, H. C. (2023). Artificial intelligence, machine learning and neural networks for tomography in smart grid - performance comparison between topology identification methodology and neural network identification methodology for the distribution line and branch line length approximation of overhead low-voltage broadband over power lines network topologies. *Trends in Renewable Energy, 9,* 34-77. doi: https://doi.org/10.17737/tre.2023.9.1.00149

[3]   Yu, F. R., Zhang, P., Xiao, W., & Choudhury, P. (2011). Communication systems for grid integration of renewable energy resources. *IEEE Network, 25*, 22-29.

[4]   Hallak, G., Berners, M., & Mengi, A. (2021). Planning tool for fast roll-out of G.hn broadband PLC in smart grid networks: Evaluation and field results. *In 2021 IEEE International Symposium on Power Line Communications and its Applications (ISPLC),* Aachen, Germany, 2021, pp. 108-113, doi: https://doi.org/10.1109/ISPLC52837.2021.9628557.

[5]   Aalamifar, F., & Lampe, L. (2017). Optimized WiMAX profile configuration for smart grid communications. *IEEE Transactions on Smart Grid, 8*(6), 2723-2732.

[6]   Lazaropoulos, A. G. (2014). Wireless sensor network design for transmission line monitoring, metering and controlling introducing broadband over powerlines-enhanced network model (BPLeNM). *ISRN Power Engineering, 2014,* Article ID 894628, 22 pages. doi: https://doi.org/10.1155/2014/894628.

[7]   Rehmani, M. H., Reisslein, M., Rachedi, A., Erol-Kantarci, M., & Radenkovic, M. (2018). Integrating renewable energy resources into the smart grid: recent developments in information and communication technologies. *IEEE Transactions on Industrial Informatics, 14(7)*, 2814-2825.

[8]   Heile, B. (2010). Smart grids for green communications [industry perspectives]. *IEEE Wireless Communications, 17*(3), 4-6.

[9]   Lazaropoulos, A. G. (2020). Statistical Channel Modeling of Overhead Low Voltage Broadband over Power Lines (OV LV BPL) Networks - Part 1: The Theory of Class Map Footprints of Real OV LV BPL Topologies, Branch Line Faults and Hook-Style Energy Thefts. *Trends in Renewable Energy, 6*, 61-87. doi: https://doi.org/10.17737/tre.2020.6.1.0011

[10]   Lazaropoulos, A. G., & Leligou, H. C. (2022). Fiber optics and broadband over power lines in smart grid: a communications system architecture for overhead high-voltage, medium-voltage and low-voltage power grids. *Progress in Electromagnetics Research B, 95,* 185-205. doi: https://doi.org/10.2528/PIERB22062502

[11]   Lazaropoulos, A. G., & Cottis, P. G. (2009, July). Transmission Characteristics of Overhead Medium-Voltage Power-Line Communication Channels. *IEEE Transactions on Power Delivery, 24*(3), 1164-1173. doi: https://doi.org/10.1109/tpwrd.2008.2008467

[12]   Lazaropoulos, A. G., & Cottis, P. G. (2010). Broadband transmission via underground medium-voltage power lines—Part I: Transmission characteristics. *IEEE Transactions on Power Delivery, 25*(4), 2414-2424. doi: https://doi.org/10.1109/TPWRD.2010.2073829

[13]   Lazaropoulos, A. G. (2012). Towards modal integration of overhead and underground low-voltage and medium-voltage power line communication channels in the smart grid landscape: Model expansion, broadband signal transmission characteristics, and statistical performance metrics (Invited paper). *ISRN Signal Processing, 2012,* 1-17. doi: https://doi.org/10.1155/2012/121628

[14]   Versolatto, F., & Tonello, A. M. (2011). An MTL theory approach for the simulation of MIMO power-line communication channels. *IEEE Transactions on Power Delivery, 26*(3), 1710-1717. doi: https://doi.org/10.1109/TPWRD.2011.2158829

[15]   Amirshahi, P., & Kavehrad, M. (2006). High-frequency characteristics of overhead multiconductor power lines for broadband communications. *IEEE*

Journal on Selected Areas in Communications, 24(7), 1292-1303. doi: https://doi.org/10.1109/JSAC.2006.061003

[16]   Stadelmeier, L., Schneider, D., Schill, D., Schwager, A., & Speidel, J. (2008). MIMO for inhome power line communications. In *Proceedings of the International Conference on Source and Channel Coding*, Ulm, Germany.

[17]   Sartenaer, T. (2004). *Multiuser communications over frequency selective wired channels and applications to the powerline access network*. Doctoral dissertation, Université catholique de Louvain, Louvain-la-Neuve, Belgium.

[18]   Galli, S., & Banwell, T. (2006). A deterministic frequency-domain model for the indoor power line transfer function. *IEEE Journal on Selected Areas in Communications,   24*(7),   1304-1316.   doi: https://doi.org/10.1109/JSAC.2006.061004

[19]   Galli, S., & Banwell, T. (2005). A novel approach to accurate modeling of the indoor power line channel—Part II: Transfer function and channel properties. *IEEE Transactions on Power Delivery, 20*(3), 1869-1878. doi: https://doi.org/10.1109/TPWRD.2005.853011

[20]   Pérez, A., Sánchez, A. M., Regué, J. R., Ribó, M., Aquilué, R., Rodríguez-Cepeda, P., & Pajares, F. J. (2009). Circuital and modal characterization of the power-line network in the PLC band. *IEEE Transactions on Power Delivery, 24*(3), 1182-1189. doi: https://doi.org/10.1109/TPWRD.2009.2021028

[21]   Sartenaer, T., & Delogne, P. (2006). Deterministic modeling of the (shielded) outdoor powerline channel based on the multiconductor transmission line equations. *IEEE Journal on Selected Areas in Communications, 24*(7), 1277-1291. doi: https://doi.org/10.1109/JSAC.2006.070804

[22]   Sartenaer, T., & Delogne, P. (2001). Powerline cables modeling for broadband communications. In *Proceedings of the IEEE International Conference on Power Line Communications and Its Applications*. Malmö, Sweden, pp. 331-337.

[23]   Paul, C. R. (1994). *Analysis of multiconductor transmission lines*. New York: John Wiley & Sons.

[24]   Meng, H., Chen, S., Guan, Y. L., Law, C. L., So, P. L., Gunawan, E., & Lie, T. T. (2004). Modeling of transfer characteristics for the broadband power line communication channel. *IEEE Transactions on Power Delivery, 19*(3), 1057-1064. doi: https://doi.org/10.1109/TPWRD.2004.827519

[25]   Lazaropoulos, A. G. (2019). Statistical broadband over power lines channel modeling - Part 1: The theory of the statistical hybrid model. *Progress in Electromagnetics Research C, 92*, 1-16.

[26]   Qu, B., Wang, H., Chen, Z., Zheng, Z., Han, Z., & Zhang, L. (2021). A channel selection algorithm of power line communication network base on double-layer cascade artificial neural network. *IOP Publishing Journal of Physics: Conference Series, 2031*(1), 012041.

[27]   Lazaropoulos, A. G. (2017). Improvement of Power Systems Stability by Applying Topology Identification Methodology (TIM) and Fault and Instability Identification Methodology (FIIM) - Study of the Overhead Medium-Voltage Broadband over Power Lines (OV MV BPL) Networks Case. *Trends in Renewable Energy, 3*(2), 102-128. doi: https://doi.org/10.17737/tre.2017.3.2.0034

[28]   Lazaropoulos, A. G. (2016). Measurement Differences, Faults and Instabilities in Intelligent Energy Systems - Part 1: Identification of Overhead High-Voltage Broadband over Power Lines Network Topologies by Applying Topology

Identification Methodology (TIM). *Trends in Renewable Energy, 2*, 85-112. doi: https://doi.org/10.17737/tre.2016.2.3.0026

[29] Lazaropoulos, A. G. (2016). Measurement Differences, Faults and Instabilities in Intelligent Energy Systems - Part 2: Fault and Instability Prediction in Overhead High-Voltage Broadband over Power Lines Networks by Applying Fault and Instability Identification Methodology (FIIM). *Trends in Renewable Energy, 2*, 113-142. doi: https://doi.org/10.17737/tre.2016.2.3.0027

[30] Lazaropoulos, A. G. (2016). Best L1 piecewise monotonic data approximation in overhead and underground medium-voltage and low-voltage broadband over power lines networks: Theoretical and practical transfer function determination. *Hindawi Journal of Computational Engineering, 2016*, 6762390, 24 pp. doi: https://doi.org/10.1155/2016/6762390

[31] Lazaropoulos, A. G. (2017). Power Systems Stability through Piecewise Monotonic Data Approximations - Part 1: Comparative Benchmarking of L1PMA, L2WPMA and L2CXCV in Overhead Medium-Voltage Broadband over Power Lines Networks. *Trends in Renewable Energy, 3*, 2-32. doi: https://doi.org/10.17737/tre.2017.3.1.0029

[32] Lazaropoulos, A. G. (2017). Power Systems Stability through Piecewise Monotonic Data Approximations - Part 2: Adaptive Number of Monotonic Sections and Performance of L1PMA, L2WPMA, and L2CXCV in Overhead Medium-Voltage Broadband over Power Lines Networks. *Trends in Renewable Energy, 3*, 33-60. doi: https://doi.org/10.17737/tre.2017.3.1.0030

[33] Lazaropoulos, A. G. (2017). Main Line Fault Localization Methodology in Smart Grid - Part 2: Extended TM2 Method, Measurement Differences and L1 Piecewise Monotonic Data Approximation for the Overhead Medium-Voltage Broadband over Power Lines Networks Case. *Trends in Renewable Energy, 3*, 26-61. doi: https://doi.org/10.17737/tre.2017.3.3.0037

[34] Lazaropoulos, A. G., & Cottis, P. G. (2013). Review and progress towards the capacity boost of overhead and underground medium-voltage and low-voltage broadband over power lines networks: Cooperative communications through two- and three-hop repeater systems. *ISRN Electronics, 2013*, 472190.

[35] Lazaropoulos, A. G., & Cottis, P. G. (2010). Capacity of overhead medium voltage power line communication channels. *IEEE Transactions on Power Delivery, 25*(2), 723-733. doi: https://doi.org/10.1109/TPWRD.2009.2038119

[36] Lazaropoulos, A. G., & Cottis, P. G. (2010). Broadband transmission via underground medium-voltage power lines-Part II: capacity. *IEEE Transactions on Power Delivery, 25*(4), 2425-2434. doi: https://doi.org/10.1109/TPWRD.2010.2070829

[37] Opera1, D44. (2005). *Report presenting the architecture of PLC system, the electricity network topologies, the operating modes and the equipment over which PLC access system will be installed*. IST Integrated Project No 507667. December.

[38] Amirshahi, P. (2006). *Broadband access and home networking through powerline networks*. Ph.D. dissertation, Pennsylvania State University, University Park, PA.

[39] D'Amore, M., & Sarto, M. S. (1997). A new formulation of lossy ground return parameters for transient analysis of multiconductor dissipative lines. *IEEE Transactions on Power Delivery, 12*, 303-314.

[40] D'Amore, M., & Sarto, M. S. (1996). Simulation models of a dissipative transmission line above a lossy ground for a wide-frequency range-Part I: Single conductor configuration. *IEEE Transactions on Electromagnetic Compatibility, 38*, 127-138.

[41] D'Amore, M., & Sarto, M. S. (1996). Simulation models of a dissipative transmission line above a lossy ground for a wide-frequency range-Part II: Multi-conductor configuration. *IEEE Transactions on Electromagnetic Compatibility, 38*, 139-149.

[42] Lazaropoulos, A. G. (2018). Broadband Performance Metrics and Regression Approximations of the New Coupling Schemes for Distribution Broadband over Power Lines (BPL) Networks. *Trends in Renewable Energy, 4*, 43-73. doi: https://doi.org/10.17737/tre.2018.4.1.0059

[43] Lazaropoulos, A. G. (2016). New coupling schemes for distribution broadband over power lines (BPL) networks. *Progress in Electromagnetics Research B, 71*, 39-54.

[44] Lazaropoulos, A. G. (2020). Business Analytics and IT in Smart Grid - Part 1: The Impact of Measurement Differences on the iSHM Class Map Footprints of Overhead Low-Voltage Broadband over Power Lines Topologies. *Trends in Renewable Energy, 6*, 156-186. doi: https://doi.org/10.17737/tre.2020.6.2.00117

[45] Lazaropoulos, A. G. (2017). Main Line Fault Localization Methodology in Smart Grid - Part 1: Extended TM2 Method for the Overhead Medium-Voltage Broadband over Power Lines Networks Case. *Trends in Renewable Energy, 3*, 2-25. doi: https://doi.org/10.17737/tre.2017.3.3.0036

[46] Lazaropoulos, A. G. (2012). Deployment concepts for overhead high voltage broadband over power lines connections with two-hop repeater system: Capacity countermeasures against aggravated topologies and high noise environments. *Progress in Electromagnetics Research B, 44*, 283-307.

[47] Okoh, D. (2016). *Computer Neural Networks on MATLAB.* CreateSpace Independent Publishing Platform.

[48] Okoh, D. (2023). *Neural Network Training Code* (https://www.mathworks.com/matlabcentral/fileexchange/59362-neural-network-training-code), MATLAB Central File Exchange. Accessed on November 17, 2023.

[49] Ibnkahla, M. (2020). Applications of neural networks to digital communications-a survey. *Signal processing, 80*(7), 1185-1215.

[50] Ma, Y. T., Liu, K. H., & Guo, Y. N. (2008). Artificial neural network modeling approach to power-line communication multi-path channel. In *Proceedings of the International Conference on Neural Networks and Signal Processing*, pp. 229-232.

[51] Hecht-Nielsen, R. (1992). Theory of the backpropagation neural network. In *Neural networks for perception*. Academic Press, pp. 65-93.

[52] Lazaropoulos, A. G., & Leligou, H. C. (2024). Big Data and Neural Networks in Smart Grid - Part 2: The Impact of Piecewise Monotonic Data Approximation Methods on the Performance of Neural Network Identification Methodology for the Distribution Line and Branch Line Length Approximation of Overhead Low-Voltage Broadband over Powerlines Networks. *Trends in Renewable Energy, 10*, 67-97. doi: https://doi.org/10.17737/tre.2024.10.1.00165

[53] Demetriou, I. C., & Powell, M. J. D. (1991). Least squares smoothing of univariate data to achieve piecewise monotonicity. *IMA Journal of Numerical Analysis, 11*(4), 411-432.

[54] Demetriou, I. C., & Koutoulidis, V. (2013). On signal restoration by piecewise monotonic approximation. In *Proceedings of the World Congress on Engineering 2013*, London, UK (July 2013), pp. 268-273.

[55] Demetriou, I. C. (1994). Best L1 piecewise monotonic data modelling. *International Transactions on Operational Research, 1*, 85-94.

[56] Demetriou, I. C. (2013). An application of best *L*1 piecewise monotonic data approximation to signal restoration. *IAENG International Journal of Applied Mathematics, 53*, 226-232.

[57] Demetriou, I. C. (2003). L1PMA: A Fortran 77 package for best L1 piecewise monotonic data smoothing. *Computer Physics Communications, 151*, 315-338.

[58] Demetriou, I. C. (2022). A binary search algorithm for univariate data approximation and estimation of extrema by piecewise monotonic constraints. *Journal of Global Optimization, 82*, 691-726.

[59] Vassiliou, E. E., & Demetriou, I. C. (2022). Piecewise monotonic data approximation: Spline representation and linear model-basic statistics. *IAENG International Journal of Applied Mathematics, 52(1)*, March 2022.